2005

Adaptive backstepping based nonlinear control of an interior permanent magnet synchronous motor drive

Lau, Jason W.

NOTE TO USERS

Page(s) not included in the original manuscript and are unavailable from the author or university. The manuscript was scanned as received.

ii

This reproduction is the best copy available.

UMI®

ADAPTIVE BACKSTEPPING BASED NONLINEAR CONTROL OF AN INTERIOR PERMANENT MAGNET SYNCHRONOUS MOTOR DRIVE

By

Jason Lau

SUBMITTED IN PARTIAL FULFILLMENT OF THE
REQUIREMENTS FOR THE DEGREE OF
MASTER OF SCIENCE
AT
LAKEHEAD UNIVERSITY
THUNDER BAY, ONTARIO
OCTOBER 2005

Your file Votre référence
ISBN: 978-0-494-15626-1
Our file Notre référence
ISBN: 978-0-494-15626-1

Table of Contents

Acknowledgements

I would like to sincerely thank my supervisor Dr. M. Nasir Uddin for his guidance and encouragement throughout the program. This work would not have been possible without his support. I would also like to thank the Faculty of Engineering at Lakehead University, faculty members, staff members and my fellow graduate students for their support throughout the program.

Finally, I would like to thank my parents and Emily Lau for their patience.

Abstract

Permanent magnet synchronous machines (PMSM) have shown increasing popularity in recent years for industrial drive applications due to the recent developments in magnetic materials, power converters, and digital signal processors. In particular, Interior Permanent Magnet Synchronous Motor (IPMSM) drives are widely used in high performance drive (HPD) applications. Fast and accurate speed response and quick recovery of speed from any disturbances are essential. The control of a high performance permanent magnet synchronous motor drive for general industrial application has received wide spread interest of researchers.

In this work, a novel speed and position control scheme for an IPMSM is developed based on a nonlinear adaptive control scheme. The vector control scheme is used to simplify control of the IPMSM. System model equations are represented in the synchronously rotating reference frame and provide the basis for the controller which is designed using the adaptive backstepping technique. Using Lyapunov's stability theory, it is also shown that the control variables are asymptotically stable. The complete system model is developed and then simulated using MATLAB/Simulink software. Performance of the proposed controller is investigated extensively at different dynamic operating conditions such as sudden load change, command speed change, command position change and parameter variations. The results show the global stability of the proposed

controller and hence found to be suitable for high performance industrial drive applications. The real time implementation of the complete drive system is currently underway.

List of Acronyms

ABNL	Adaptive Backstepping based Nonlinear Controller
BLDC	Brushless DC
DSP	Digital signal processor
HPD	High Performance Drive
IPMSM	Interior Permanent Magnet Synchronous Motor
MRAC	Model Reference Adaptive Controller
PI	Proportional Integral
PID	Porportional Integral Derivative
PM	Permanent Magnet
PMSM	Permanent Magnet Synchronous Motor
PWM	Pulse Width Modulation
RTI	Real Time Interface
SMC	Sliding Mode Control
TI	Texas Instruments
VSI	Voltage Source Inverter

List of Symbols

v_a,v_b,v_c	a, b and c phase voltages
v_a^*,v_b^*,v_c^*	command a, b and c phase voltages
i_a,i_b,i_c	a, b and c phase currents
v_d	d-axis voltage
v_q	q-axis voltage
i_d	d-axis current
i_q	q-axis current
i_q^*	q-axis command current
R	stator resistance per phase
L_d	d-axis inductance
L_q	q-axis inductance
L_{md}	d-axis magnetizing inductance
L_{mq}	q-axis magnetizing inductance
ω_r	rotor speed
ω_r^*	motor command speed
θ_r	rotor position
θ_r^*	motor command position
p	differential operator $\frac{d}{dt}$
P	number of pole pairs

T_e	developed electromagnetic torque
T_L	load torque
J	rotor inertia constant
B_m	friction damping coefficient
ψ_m	magnet flux linkage
V_B	dc bus voltage for the inverter

Chapter 1

Introduction

For many years, DC motors were used for variable speed and high performance drive applications because of the simplicity of control due to the decoupled nature of the field and armature [1]. However, disadvantages of dc motors include, lack of overload capability, lack of ruggedness, frequent maintenance requirement as well as high cost due to brush-gear and commutators, and power loss in the field circuit. These drawbacks have encouraged researchers to develop ac motors such as induction and synchronous motors for high performance variable speed drive applications, where robustness and maintenance free operations are the main concern.

The induction motor is the most commonly used in industry due to its ruggedness, reliability and low cost [2, 3]. However, they have some limitations associated with their use in high performance variable speed drive applications. One of the limitations is that induction motors always operate at lagging power factor because their rotor induced current is supplied from the stator side. Also, the induction motor always runs at speeds lower than the synchronous speed, so the control of these motors is very complex. The real

time implementation of the induction motor drive requires sophisticated modeling and estimation of machine parameters with complex control circuitry. Due to these limitations, researchers have looked into the synchronous motors for easier control in high performance variable speed drives.

Synchronous motors of wire-wound rotor type are common in high power ac drive systems because the field current can be controlled from the rotor side. Since it runs at synchronous speed, the control is less complex. It also removes the slip power loss. However, the presence of the field coil, dc supply and slip rings decrease the efficiency of the drive and requires frequent maintenance. Due to the significant technological advancement that has occurred in motor drives in recent years, the permanent magnet synchronous motor is becoming increasingly popular in varied drive applications [4, 5].

1.1 Permanent Magnet Synchronous Motors

A permanent magnet synchronous motor consists of a stator with three phase windings and a rotor mounted with permanent magnets to provide the field flux. The permanent magnet synchronous motor is not subjected to the limitations of dc, ac induction and wire-wound excited synchronous motors as previously discussed. It does not need an external supply to excite the rotor field and hence the field winding and slip rings are eliminated. The absence of the field winding reduces the cost and eliminates the power losses associated with this winding. The permanent magnet synchronous motor occupies less space than a wire-wound motor for a given size, which leads to more compact design and robust construction. Unlike an induction motor there is no slip dependent rotor copper loss in a permanent magnet synchronous motor. The permanent magnet synchronous motor is more efficient and has a larger torque

to inertia ratio and power density when compared to the induction motor. In addition, for the same output capacity the PMSM is smaller in size and lower in weight. This is preferable for certain high performance applications like in machine tools and aerospace [6].

1.2 Classification of PMSM

PM synchronous motors are classified in different categories depending on the position of the magnets within the rotor. The categories are:

- Surface mounted where the magnets are mounted on the surface of the rotor.
- Inset type where the permanent magnets are are fully or partially inset into the rotor core
- Interior type where the magnets are buried within the rotor core.

The cross section of the different types of PM motors are shown in Figures 1.1 - 1.3. The motor with surface magnets is essentially non-salient type. It has a large air gap and is popularly used in a brushless dc motor drive as for example in a washer/dryer or computer hard disk drives. The large air gap weakens the armature reaction effect, and therefore the operation is essentially restricted to low speed and constant torque region. The inset permanent magnet motor has a small but relatively smooth air gap. The interior permanent magnet motor overcomes the above drawbacks of surface magnet type because of its narrow and smooth air gap. Moreover, the motor torque is contributed by reluctance component due to the difference between direct and quadrature axis reactances as well as the permanent magnet field component. Unlike

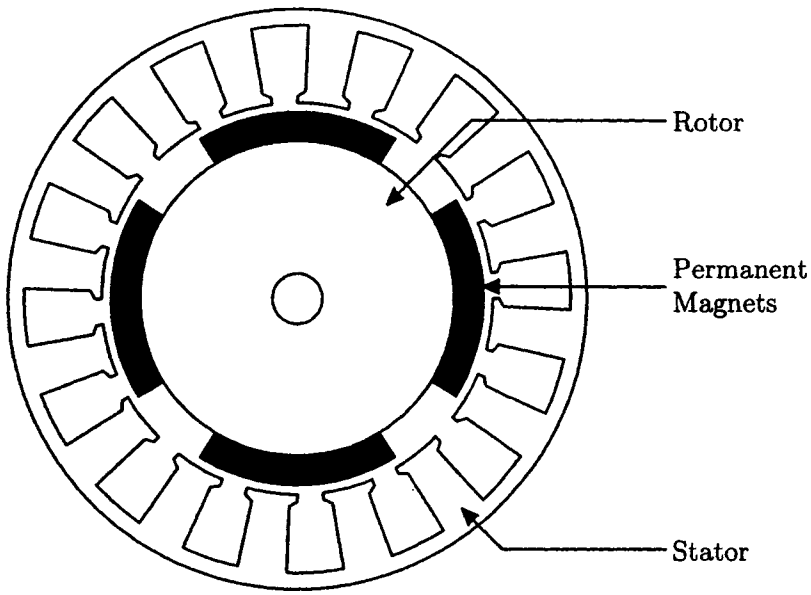

Figure 1.1: Cross section of surface mounted type PM motor

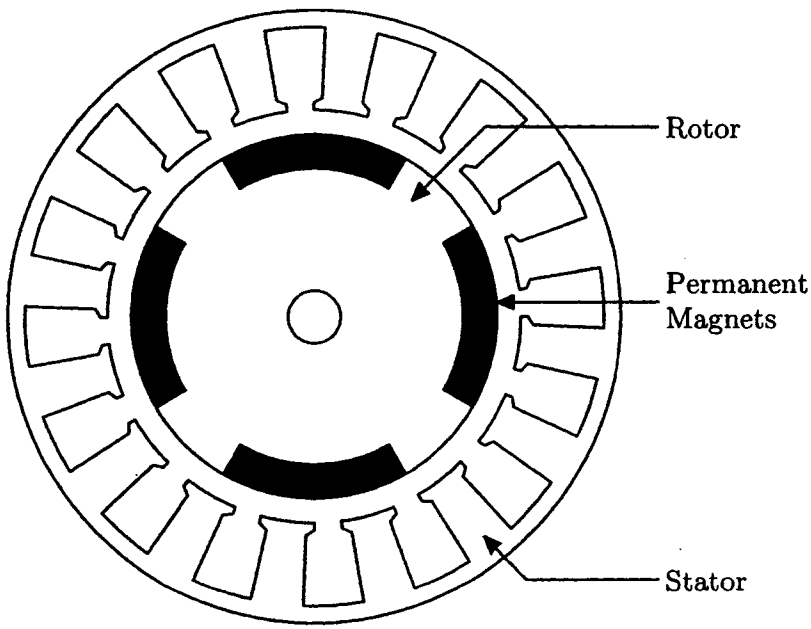

Figure 1.2: Cross section of inset type PM motor

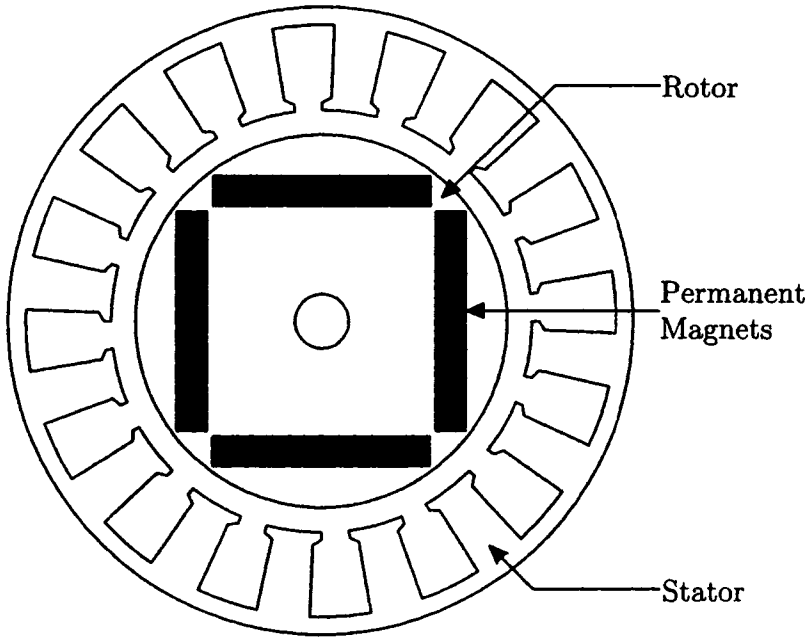

Figure 1.3: Cross section of interior type PM motor

surface mounted magnet type, it has advantages for high-speed applications. Depending on the rotor cage winding, the PM motors may be classified as: (a) cageless, where the rotor has no cage winding and (b) cage type, where the rotor is provided with a cage winding. In the case of the cage type motor, the cage winding provides the starting torque and hence this type of motor is capable of self-starting with a rated supply voltage and frequency [7].

Among the various types of PM motors discussed above, the interior type PM motor is the most economical to manufacture. Since the permanent magnets are buried within the rotor core, it provides a smooth rotor surface and reduced air gap. As a result, this type of motor can be used for high speed with quiet operation and better dynamic performance, which are the major concerns for high performance drive systems. In order to take all of these

advantages without the lack of generality, the interior permanent magnet synchronous motor (IPMSM) has been considered as a working model in this thesis.

1.3 Literature Review

Developments in PM motor technology is directly related to advances in permanent magnet materials such as ferrites, AlNiCo, rare earths such as Samarium Cobalt (SmCo) and Neodymium-Iron-Boron (NdFeB) [8]. Typical residual flux densities of these PM materials are 1.1 T for neodymium, 0.85 T for samarium cobalt and 0.35 T for ferrites [4]. Advances in semiconductor and microprocessor technologies have made evolutionary advancements on the design and control of electric motors. Ac drives have already begun to replace the dc motors in motion control applications and possibly make dc motors relatively obsolete in the next few years. The dynamics and control of ac drives are complex, and their complexity increases for higher performance requirements. Many different control techniques of varying degree of complexity have appeared on the nature of drive applications.

The simple open-loop volt/hertz (v/f) control method has been popularly used for a long time in low performance drives. Other methods include torque control, current angle control and flux control. However, these scalar control techniques have drawbacks due to the nonlinearity of the motor model and inherent coupling between the direct and quadrature axis (d-q axis) quantities. This causes sluggish responses which are unacceptable for high-performance drive applications which require fast and accurate speed tracking response, quick recovery of speed from any disturbances and must be insensitive to parameter variations. In order to achieve these required characteristics of

hight performance drives the vector or field oriented control technique is being utilized for control of ac drives [9].

The principle of vector control is to eliminate the coupling between the direct (d) and quadrature (q) axes. Both the phase angle and the magnitude of the current must be controlled. This is achieved by transforming the abc quantities into the d-q quantities using Park's transformation [10]. The ac motor then behaves like a separately excited dc motor while maintaining the advantages of ac over dc motors. Thus, the control of ac motors becomes easier as the q-axis component of the current affects the torque while the d-axis current only affects the magnitude of the flux. This indicates a close correspondence to dc machines, with the direct axis component of the stator current vector being analogous to the field current and the quadrature axis component to the armature current.

Based on the control signals, vector control is classified as direct and indirect methods. The direct method depends on the direct measurements of the stator (or rotor) flux, whereas the indirect method involves calculating the necessary variables from information of the rotor position.

1.3.1 Adaptive Speed and Position Control

The controllers used in motor drive systems can be broadly classified as fixed gain types or adaptive types. The conventional fixed gain types are proportional-integral (PI), proportional-integral-derivative (PID) and pseudo-derivative-feedback (PDF) controllers. Fixed gain controllers are sensitive to parameter variations due to saturation, temperature variation, sudden change of command speed, load disturbances and other uncertainties [11]. Therefore, these types of controllers are not always suitable for high performance applications.

To overcome these obstacles, researchers [11–26] have developed adaptive control schemes so that the controller can adapt to parameter variations and load disturbances. The adaptive types are model reference adaptive controller (MRAC), sliding mode controller (SMC), self tuning regulator (STR) and variable structure controller (VSC). Major reported works on the interior permanent magnet synchronous motor (PMSM) drive will be briefly discussed below.

Various linear and non linear adaptive controllers have been proposed for IPMSM drive system. Some include LQ control, differential geometric approach, passivity theory, self tuning control, observer based adaptive control and model reference adaptive control [11–19]. In [16] the authors developed a discrete time adaptive speed controller for the PMSM where the nonlinear motor system was linearized in the discrete time domain. The mechanical parameters of the system are also estimated, however the controller is highly dependent on the accuracy of these estimated parameters. The same authors have also proposed a discrete time observer based adaptive controller without the use of speed sensors [17]. However, it was determined that observer based adaptive control is sensitive to inertial mismatch. Estimation of the motor speed required high gains in the presence of inertial mismatch. This amplifies the noise in the system which leads to poor performance. In [18] an adaptive uncertainty observer is utilized with a conventional PI controller for position control of a PMSM. This method was proven to be robust but the authors have not applied this technique for speed control. The model reference adaptive control technique has been used for speed and position control suitable for robotic applications [14]. A disturbance torque observer is employed to balance the required load torque and reduce the complexity of the adaptive

algorithm. However, the proposed model suffers from increased on-line computational burden for increased robustness of the drive. In [15], the authors have combined model reference algorithms with variable structure algorithms for adaptive position control of a PMSM. MRAC techniques involve tuning the controller online by adaptive algorithms based on the error between the reference model and the controlled plant.

Other adaptive control techniques in speed and position control of a PMSM include sliding mode control (SMC), torque ripple minimization, efficiency maximizing, maximum torque per ampere control and self tuning control using Kalman filter theory [20–26]. Generally, to design a conventional SMC system, there are two design phases that must be considered, namely, the reaching phase and sliding phase. The robustness of a variable structure control (VSC) system resides in its sliding phase, but not in its reaching phase. In other words, the closed-loop system dynamic is not completely robust all the time. In addition, while the design technique for the sliding mode has been well established, there is no easy way to shape the dynamics of the reaching phase [20,21]. In [27] the authors have reported an ac servo drive for PMSM using a variable structure controller. They have used two control loops: the inner loop is used for predictive current controllers and the outer loop is used for a position or speed controller. The predictive current controller has been used to improve the robustness of the drive. However, the performance of the drive has not been investigated for wide range of speed conditions. Moreover, the drive is not completely rid of the chattering problem even in the steady state. The authors of [22] have combined sliding mode control with fuzzy logic rules to reduce chattering and improve steady state error which is associated with SMC. Bin Zhang et. al [28] have also combined a sliding mode controller

based on model reference adaptive control. Combining different control techniques gives superior results to conventional fixed gain controllers, however they increase the computational complexity of the control algorithm.

1.3.2 Adaptive Backstepping

Backstepping control is a relatively new technique for the control of uncertain nonlinear systems. The most appealing point is the use of virtual control variables to make the original high order system simple, thus the final control outputs can be derived step by step through suitable Lyapunov functions ensuring global stability. An adaptive robust nonlinear controller can be derived using this control method in a straightforward manner.

Recently, the newly developed adaptive backstepping technique has been used in the design of speed controllers for dc, induction motors and permanent magnet motors [29–36]. This technique allows the designer to incorporate most system non linearities and uncertainties in the design of the controller. In [30, 31, 33] the authors designed a nonlinear controller that achieves rotor angular speed and rotor flux amplitude tracking with uncertainties in the rotor resistance and load torque for an induction motor. Results show that tracking objectives are achieved with very little steady state error or overshoot. Zhou et. al [29] have developed a backstepping based controller for a DC motor and induction motor with uncertainties. First, the authors derived a nonlinear model of a DC motor with parameter uncertainties such as motor inertia and load torque. Then the control algorithm is derived from the model equations. Hualin Tan et.al [32] have also designed an adaptive backstepping based controller for position control of an induction motor. Once again the simulated results showed that tracking objectives were achieved. The authors

of [36] have successfully implemented a backstepping based controller in real time for an IPMSM drive system. However, in designing the controller the authors of [36] did not take into account all possible system nonlinearities such as stator resistance which varies with temperature. Stator resistance can vary as much as 70% with temperature [37].

1.4 Thesis Objectives

Based on the literature review, the IPMSM possesses many appealing characteristics, such as high torque to inertia ratio, power to weight ratio and low noise. However, due to the nonlinear nature of the motor, traditional control methods such as scalar control and fixed gain PI control are not suitable for high performance drive applications. Some works have been reported on adaptive control for the IPMSM such as MRAC, SMC etc. However, the absence of proper estimation of the motor parameters degrades the performance of these controllers. Therefore, the objective of this thesis is to develop a robust nonlinear controller for speed and position control of an IPMSM drive. The proposed method is based on the adaptive backstepping technique. Motor parameters are estimated online in order to handle system disturbances and uncertainties. The vector control scheme is used for the proposed IPMSM drive. This decouples the torque and flux, thus providing faster transient response and making the control task easier.

1.5 Thesis Organization

The organization of the remaining chapters is as follows. Chapter 2 describes Park's transformation and the derivation of the mathematical model of the

IPMSM. Here it is shown that the vector control technique greatly simplifies the control of the motor. Next, Chapter 3 shows the control design in detail for both speed and position control. The design is based on the motor model equations derived in Chapter 2. Chapter 4 describes the model development and shows the simulation results of the complete drive system. Chapter 5 describes how the real time implementation of the complete drive system would be carried out. Finally, a summary of this work and suggestions for future work are highlighted in Chapter 6. After that, all pertinent references and appendices are listed.

Chapter 2

Mathematical Model of the IPMSM

2.1 Park's Transformation

In order to simplify the mathematical model of the motor it will be expressed in terms of the synchronously rotating reference frame where the machine equations are no longer dependent on rotor position. This transformation is also known as Park's Transformation [10]. First the machine equations are to be transformed from the stationary *abc* frame to the stationary $d^s - q^s$ frame. Then the second step is from the stationary $d^s - q^s$ frame to the synchronously rotating $d^r - q^r$ frame. The *abc* phase quantities can be transformed into the stationary $dq0$ axis quantities using the following equation.

$$\begin{bmatrix} x_q^s \\ x_d^s \\ x_0^s \end{bmatrix} = \frac{2}{3} \begin{bmatrix} \cos\theta_r & \cos\left(\theta_r - \frac{2\pi}{3}\right) & \cos\left(\theta_r + \frac{2\pi}{3}\right) \\ \sin\theta_r & \sin\left(\theta_r - \frac{2\pi}{3}\right) & \sin\left(\theta_r + \frac{2\pi}{3}\right) \\ \frac{1}{2} & \frac{1}{2} & \frac{1}{2} \end{bmatrix} \begin{bmatrix} x_a \\ x_b \\ x_c \end{bmatrix} \tag{2.1}$$

where x_q^s, x_d^s, x_0^s are the stationary frame $dq0$ axis quantities and x_{abc} are the abc quantities. The corresponding inverse relation is given by:

$$\begin{bmatrix} x_a \\ x_b \\ x_c \end{bmatrix} = \begin{bmatrix} \cos\theta_r & \sin\theta_r & 1 \\ \cos\left(\theta_r - \frac{2\pi}{3}\right) & \sin\left(\theta_r - \frac{2\pi}{3}\right) & 1 \\ \cos\left(\theta_r + \frac{2\pi}{3}\right) & \sin\left(\theta_r + \frac{2\pi}{3}\right) & 1 \end{bmatrix} \begin{bmatrix} x_q^s \\ x_d^s \\ x_0^s \end{bmatrix} \tag{2.2}$$

The rotor position angle is defined as

$$\theta_r = \int_0^t \omega_r(t)\, dt + \theta_r(0) \tag{2.3}$$

For a balanced 3-phase system, x_0 does not exist. Also, Equations (2.1) and (2.2) are both in the stationary reference frame so $\theta_r = \theta_r(0)$ which is the angle difference between the q-axis and a-phase. It is convenient to set $\theta_r(0) = 0$ so that the q-axis coincides with the a-phase. Under these conditions, the transformation equations can be written as

$$\begin{bmatrix} x_q^s \\ x_d^s \end{bmatrix} = \begin{bmatrix} \frac{2}{3} & -\frac{1}{3} & -\frac{1}{3} \\ 0 & -\frac{1}{\sqrt{3}} & \frac{1}{\sqrt{3}} \end{bmatrix} \begin{bmatrix} x_a \\ x_b \\ x_c \end{bmatrix} \tag{2.4}$$

and

$$\begin{bmatrix} x_a \\ x_b \\ x_c \end{bmatrix} = \begin{bmatrix} 1 & 0 \\ -\frac{1}{2} & -\frac{\sqrt{3}}{2} \\ -\frac{1}{2} & \frac{\sqrt{3}}{2} \end{bmatrix} \begin{bmatrix} x_q^s \\ x_d^s \end{bmatrix} \tag{2.5}$$

The relative positions of the stationary and rotating d-q axes is shown in Figure 2.1. Now the variables in the stationary d-q frame can be converted to the synchronously rotating $d^r - q^r$ frame by:

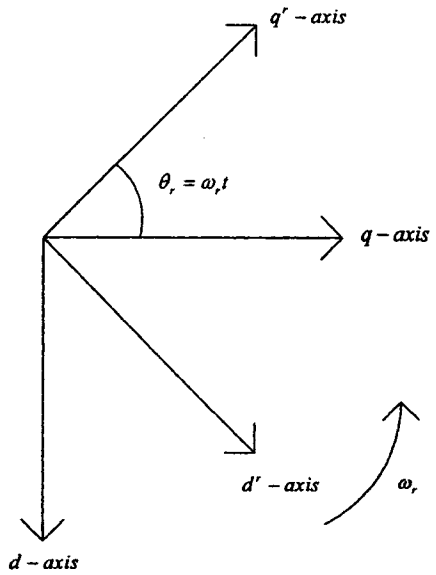

Figure 2.1: Relative positions of stationary and rotating d-q axes

$$\begin{bmatrix} x_q^r \\ x_d^r \end{bmatrix} = \begin{bmatrix} \cos\theta_r & -\sin\theta_r \\ \sin\theta_r & \cos\theta_r \end{bmatrix} \begin{bmatrix} x_q^s \\ x_d^s \end{bmatrix} \tag{2.6}$$

where x_q^r and x_d^r are the synchronously rotating reference frame quantities. The inverse relation is:

$$\begin{bmatrix} x_q^s \\ x_d^s \end{bmatrix} = \begin{bmatrix} \cos\theta_r & \sin\theta_r \\ -\sin\theta_r & \cos\theta_r \end{bmatrix} \begin{bmatrix} x_q^r \\ x_d^r \end{bmatrix} \tag{2.7}$$

In order to derive the $d^r - q^r$ model of the IPMSM drive, the following assumptions are made.

- The eddy current and hysteresis losses are negligible.
- The induced emf is sinusoidal.
- The saturation is neglected.

- The stator resistances of the three phases are balanced.

2.2 Derivation of the Motor Model

As stated before, the IPMSM is similar to the conventional wire-wound synchronous motor except the rotor excitation is provided by permanent magnets instead of wire-wound dc rotor field. Therefore, the $d-q$ axis model of the IPMSM can be derived from the standard model for synchronous motors by removing the equation related to the field current and associated dynamics. The flux linkages in the three phase stator windings due to the permanent magnets are given in matrix form as [38]:

$$\begin{bmatrix} \psi_{am} \\ \psi_{bm} \\ \psi_{cm} \end{bmatrix} = \psi_m \begin{bmatrix} \sin\theta_r \\ \sin\left(\theta_r - \frac{2\pi}{3}\right) \\ \sin\left(\theta_r + \frac{2\pi}{3}\right) \end{bmatrix} \tag{2.8}$$

where ψ_{am}, ψ_{bm} and ψ_{cm} are the a b c phase stator flux linkages due to the permanent magnet alone, ψ_m is the constant flux supplied by the permanent magnets and θ_r is the rotor position angle.

The 3-phase air gap flux linkage equations are given as:

$$\begin{bmatrix} \psi_a \\ \psi_b \\ \psi_c \end{bmatrix} = \begin{bmatrix} L_{aa} & M_{ab} & M_{ac} \\ M_{ba} & L_{bb} & M_{bc} \\ M_{ca} & M_{cb} & L_{cc} \end{bmatrix} \begin{bmatrix} i_a \\ i_b \\ i_c \end{bmatrix} + \psi_m \begin{bmatrix} \sin\theta_r \\ \sin\left(\theta_r - \frac{2\pi}{3}\right) \\ \sin\left(\theta_r + \frac{2\pi}{3}\right) \end{bmatrix} \tag{2.9}$$

where ψ_a, ψ_b and ψ_c are the 3-phase air gap flux linkages, L_{aa}, L_{bb} and L_{cc} are the self inductances and M_{ab}, M_{bc} and M_{ca} are the mutual inductances. Now

the voltage equations of the three phases of the IPMSM can be defined as

$$v_a = R_a i_a + p\psi_a \tag{2.10}$$

$$v_b = R_b i_b + p\psi_b \tag{2.11}$$

$$v_c = R_c i_c + p\psi_c \tag{2.12}$$

where v_a, v_b, v_c are the 3-phase voltages, i_a, i_b, i_c are the 3-phase currents, R_a, R_b, R_c are the 3-phase stator resistances and p is the differential operator $\frac{d}{dt}$. Now, using equations (2.10)-(2.12), the transformation equations (2.1) and (2.6) the model of the IPMSM can be written in the synchronously rotating d-q frame as

$$v_d^r = Ri_d^r + p\psi_d^r + \omega_s\psi_q^r \tag{2.13}$$

$$v_q^r = Ri_q^r + p\psi_q^r + \omega_s\psi_d^r \tag{2.14}$$

where $v_d^r, v_q^r, i_d^r, i_q^r, \psi_d^r, \psi_q^r$ are the d-q axis voltages, currents and flux linkages respectively, R is the stator resistance per phase and ω_s is the stator frequency. ψ_q^r and ψ_d^r can be written as

$$\psi_q^r = L_q i_q^r \tag{2.15}$$

$$\psi_d^r = L_d i_d^r + \psi_m \tag{2.16}$$

where

$$L_q = L_1 + L_{mq} \tag{2.17}$$

$$L_d = L_1 + L_{md} \tag{2.18}$$

L_d and L_q are the d-q axis inductances, L_{md} and L_{mq} are the d and q axis magnetizing inductances and L_l is the leakage inductance per phase. The stator frequency is related to the rotor frequency by

$$\omega_s = P\omega_r \tag{2.19}$$

where P is the number of pole pairs. Now the machine model can be re-written as

$$\begin{bmatrix} v_d^r \\ v_q^r \end{bmatrix} = \begin{bmatrix} R + pL_d & -P\omega_r L_q \\ P\omega_r L_d & R + pL_q \end{bmatrix} \begin{bmatrix} i_d \\ i_q \end{bmatrix} + \begin{bmatrix} 0 \\ P\omega_r \psi_m \end{bmatrix} \tag{2.20}$$

According to Equation (2.20) the motor can be represented by the equivalent circuit diagrams shown in Figure 2.2. The permanent magnet flux is represented as a constant current source I_M, since a constant field current in a wire wound synchronous machine will supply a constant flux.

The torque developed by the machine is obtained by considering the power entering the two sources in the circuit diagram. The total average power entering the sources per phase is given by [4]

$$P_{phase} = \frac{1}{2}(-P\omega_r L_q i_q^r i_d^r + P\omega_r L_d i_q^r i_d^r + P\omega_r \psi_m i_q^r) \tag{2.21}$$

Therefore, the total power developed by the machine is

$$P_{total} = \frac{3P\omega_r}{2}(\psi_m i_q + (L_d - L_q) i_d i_q) \tag{2.22}$$

Now, the developed electromagnetic torque is given by

$$T_e = \frac{P_{total}}{\omega_r} = \frac{3P}{2}(\psi_m i_q + (L_d - L_q) i_d i_q) \tag{2.23}$$

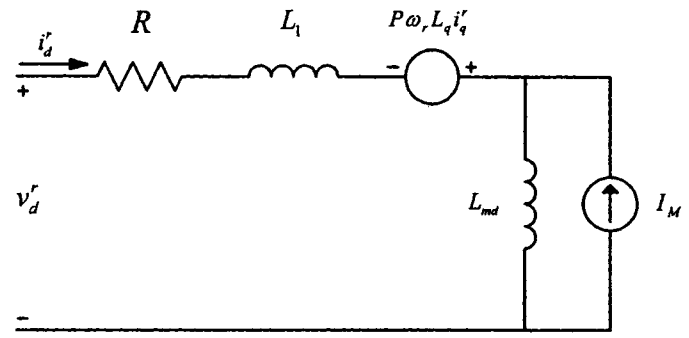

(a) d-axis equivalent circuit

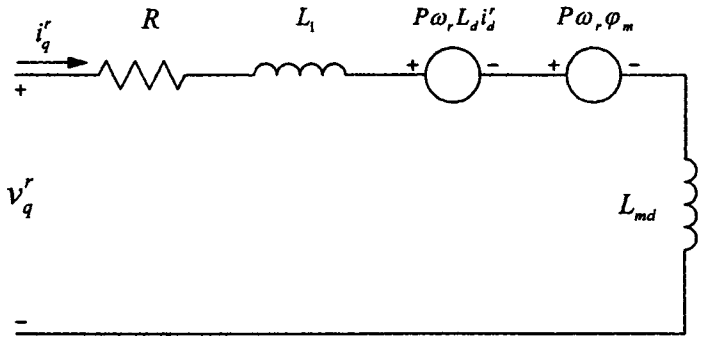

(b) q-axis equivalent circuit

Figure 2.2: Equivalent circuit model of the IPMSM

Finally, neglecting windage, the motor dynamics can be represented by the following equation:

$$T_e = T_L + J\frac{d\omega_r}{dt} + B_m\omega_r \tag{2.24}$$

where T_L is the load torque (Nm), B_m is the friction damping coefficient (Nm/rad/sec) and J is the rotor inertia constant (kgm^2). For dynamic simulation, the IPMSM model equations are expressed in state-space form as

$$\dot{i}_q = \frac{-Ri_q - P\omega_r L_d i_d - P\omega_r \psi_m + v_q}{L_q} \tag{2.25}$$

$$\dot{i}_d = \frac{-Ri_d + P\omega_r L_q i_q + v_d}{L_d} \tag{2.26}$$

$$\dot{\omega}_r = \frac{T_e - T_L - B_m\omega_r}{J} \tag{2.27}$$

2.3 Vector Control Strategy for IPMSM Drive

As discussed previously, the vector control technique is an effective technique for use with ac motors in high performance drives. The IPMSM can be vector controlled when the machine equations are transformed from the abc frame to the synchronously rotating d-q frame. The complexity of control of the IPMSM drive arises due to the nonlinear nature of the torque in equation (2.23). One way of simplifying this is to set $i_d = 0$. The torque equation then becomes

$$T_e = \frac{3P}{2}\psi_m i_q \tag{2.28}$$

which is linear and similar to the torque equation of a dc motor. Using phasor notation and taking the d^r axis as the reference phasor, the steady state phase voltage V_a can be derived from equation (2.20) as [38]

$$\begin{aligned} V_a &= v_d^r + jv_q^r \\ &= RI_a - \omega_r L_q i_q^r + j\omega_r L_d i_d^r + j\omega_r\psi_m \end{aligned} \tag{2.29}$$

where the phase current,

$$I_a = -i_d^r + ji_q^r \tag{2.30}$$

Based on equation (2.29), the basic vector diagram of the IPMSM is shown in Figure 2.3. The stator current can be controlled by by controlling the individual d-q current components. When i_d is set to zero, the torque is a function of only the q-axis current component, and hence the torque can be controlled by controlling i_q. Constant torque can be obtained by ensuring that

i_q is kept constant. Figure 2.3(b) shows the vector diagram with $i_d = 0$. With this control technique, the dynamic equations (2.25) to (2.27) can be rewritten as,

$$\dot{i}_q = \frac{-Ri_q - P\omega_r\psi_m + v_q}{L_q} \tag{2.31}$$

$$v_d^r = -P\omega_r L_q i_q \tag{2.32}$$

$$\dot{\omega}_r = \frac{T_e - T_L - B_m\omega_r}{J} \tag{2.33}$$

For the sake of testing the proposed control algorithm presented in this work, this technique is used to control the motor up to its rated speed. In order to control the motor beyond its rated speed, the flux weakening technique must be incorporated [39,40].

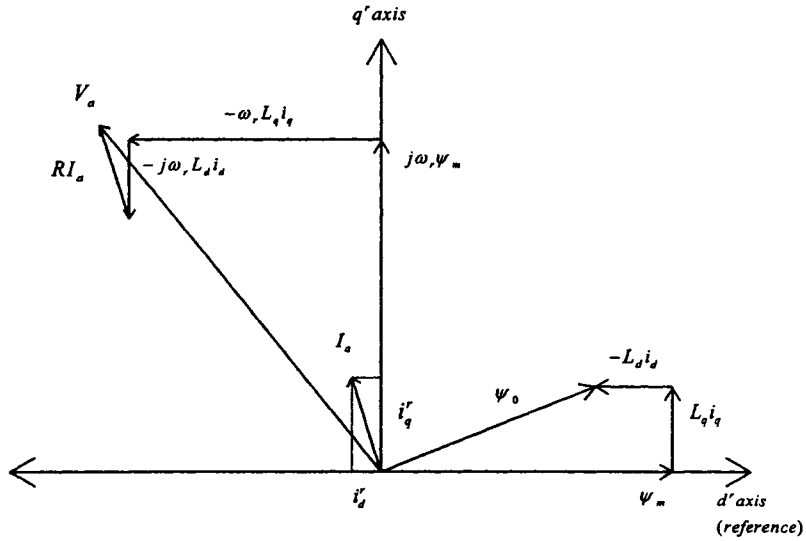

(a) General vector diagram

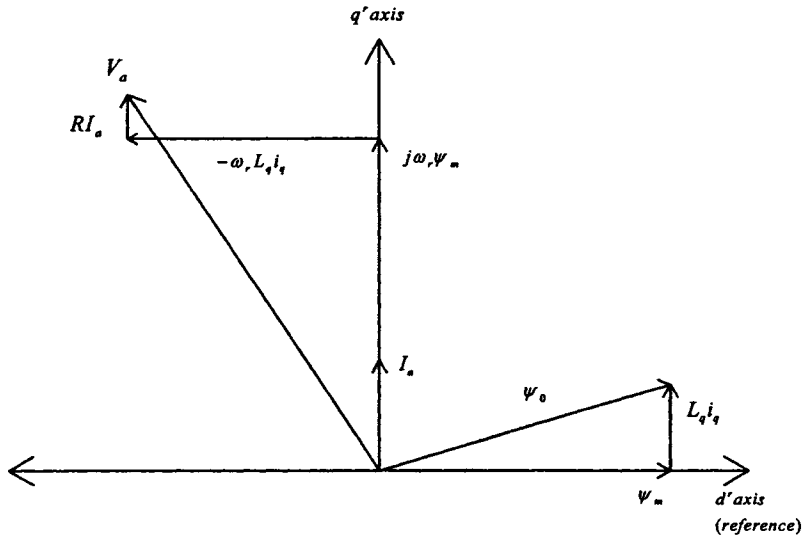

(b) Modified with $i_d = 0$

Figure 2.3: Vector diagrams of the IPMSM

Chapter 3

Adaptive Control of an IPMSM Drive

As stated before, the goal of this work is to design a speed and position controller for the IPMSM using the adaptive backstepping technique. Speed control is essential for a high performance drive application, since a motor must have a fast and accurate speed tracking response, quick recovery of speed from any disturbances and must be insensitive to parameter variations. Such applications include rolling mills, machine tools, etc.

Position control of a motor is obtained with two control loops - an outer position loop and an inner speed loop. The position controller generates the reference speed, and the speed controller generates the reference currents in the case of vector control. A typical vector control scheme for position or speed control of an IPMSM is shown in Figure 3.1. Typically, conventional controllers such as proportional integral (PI) or proportional integral derivative (PID) have been used in both loops. The main advantage to this is simplicity. However, the range of operating conditions is very limited, and the performance of the controllers degrade when uncertainties are introduced [41].

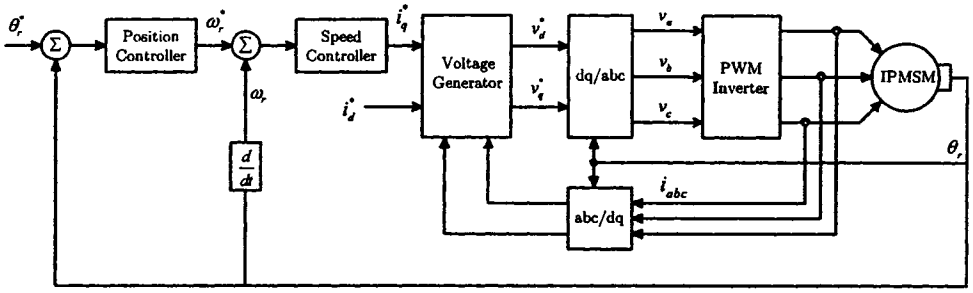

Figure 3.1: Typical vector control scheme for position or speed control of an IPMSM

In order to maintain good control performance an adaptive control scheme must be used to compensate for parameter variations [42]. Based on the motor model, the d-q axis command voltage components are generated from the command d-q axis current components. Using the inverse of Park's Transformation, the command a-b-c phase voltages are generated from the d-q axis components, and then compared with high frequency triangle waveforms to generate the PWM logic signals for the inverter.

3.1 Speed Control Design

The foundation of backstepping is the identification of a virtual control variable and forcing it to become a stabilizing function. Thus, it generates a corresponding error variable which can be stabilized by proper input selection via Lyapunov's stability theory [43]. This technique is very useful for online estimation of parameters which cannot be directly measured. Hence, this method is suitable for speed control of a nonlinear IPMSM where parameters vary with magnetic saturation such as inductance and stator resistance which varies with temperature. Moreover, the load torque is unknown and must be estimated as well for complete nonlinear adaptive control.

The overall objective is to track the rotor speed ω_r. The tracking error is given by

$$e = \omega_r^* - \omega_r \tag{3.1}$$

and the speed error dynamic is given by

$$\dot{e} = -\dot{\omega}_r = \frac{1}{J}\left[B_m\omega_r + T_L - \frac{3P}{2}\left(\psi_m i_q + (L_d - L_q)\, i_d i_q\right)\right] \tag{3.2}$$

The stabilizing function is determined by differentiating the Lyapunov function $V = \frac{1}{2}e^2$ to get

$$\dot{V} = e\dot{e} = \frac{e}{J}\left[B_m\omega_r + T_L - \frac{3P}{2}\psi_m i_q - \frac{3P}{2}\left(L_d - L_q\right) i_d i_q\right] \tag{3.3}$$

The d-q axis currents i_d and i_q are identified as the virtual control variables to stabilize motor speed. From (3.3) we choose the following stabilizing functions:

$$i_q^* = \frac{2}{3P\psi_m}\left(B_m\omega_r + T_L - k_1 Je\right) \tag{3.4}$$

$$i_d^* = 0 \tag{3.5}$$

where k_1 is a constant gain, i_q^* and i_d^* are the command currents. Substituting these equations back into equation (3.3) the Lyapunov function becomes

$$\dot{V} = -k_1 e^2 \tag{3.6}$$

if $k_1 > 0$ then the function is negative semi-definite which ensures asymptotic stability.

If the d-q axis currents are identified as the virtual control variables the corresponding error functions are defined as

$$e_q = i_q^* - i_q \tag{3.7}$$

$$e_d = i_d^* - i_d \tag{3.8}$$

Like the speed error, these error functions must also be reduced to zero. The current error dynamics are (with $i_d^* = 0$)

$$\dot{e}_d = \dot{i}_d^* - \dot{i}_d = \frac{Ri_d - P\omega_r L_q i_q - v_d}{L_d} \tag{3.9}$$

$$\dot{e}_q = \dot{i}_q^* - \dot{i}_q = \frac{2(B_m - k_1 J)}{3P\psi_m J}[T_e - B_m\omega_r - T_L] + \frac{Ri_q + P\omega_r L_d i_d + P\omega_r \psi_m - v_q}{L_q} \tag{3.10}$$

The parameters that must be estimated here are the inductances L_d and L_q which vary with magnetic saturation, stator resistance R which varies with temperature, and load torque which sometimes cannot be measured directly. The corresponding error variables are given by

$$\tilde{L}_d = \hat{L}_d - L_d;\ \tilde{L}_q = \hat{L}_q - L_q$$

$$\tilde{T}_L = \hat{T}_L - T_L;\ \tilde{R} = \hat{R} - R \tag{3.11}$$

To reduce these estimation errors to zero, another Lyapunov function is defined as

$$V_1 = \frac{1}{2}\left(e^2 + e_d^2 + e_q^2 + \frac{1}{\theta_1}\tilde{L}_d^2 + \frac{1}{\theta_2}\tilde{L}_q^2 + \frac{1}{\theta_3}\tilde{T}_L^2 + \frac{1}{\theta_4}\tilde{R}^2\right) \tag{3.12}$$

where θ_{1-4} are constant gains. Before differentiating, the speed error dynamics (3.2) and q-axis command current (3.4) must be modified to incorporate the

estimated load torque.

$$\hat{i}_q^* = \frac{2}{3P\psi_m}\left(B_m\omega_r + \hat{T}_L - k_1 Je\right) \tag{3.13}$$

where $\hat{T}_L$ is the estimated value of load torque. Now from equations (3.7),(3.8) and (3.13) the speed error dynamics is given by

$$\dot{e} = \frac{1}{J}\left[-\tilde{T}_L + \frac{3P}{2}\psi_m e_q + \frac{3P}{2}\left(L_d - L_q\right)e_d i_q - k_1 Je\right] \tag{3.14}$$

Now (3.12) can be differentiated to obtain

$$\begin{aligned}
\dot{V}_1 &= e\dot{e} + e_d\dot{e}_d + e_q\dot{e}_q + \frac{1}{\theta_1}\tilde{L}_d\dot{\tilde{L}}_d + \frac{1}{\theta_2}\tilde{L}_q\dot{\tilde{L}}_q + \frac{1}{\theta_3}\tilde{T}_L\dot{\tilde{T}}_L + \frac{1}{\theta_4}\tilde{R}\dot{\tilde{R}} \\
&= \frac{e}{J}\left[-\tilde{T}_L + \frac{3P}{2}\psi_m e_q + \frac{3P}{2}\left(L_d - L_q\right)e_d i_q - k_1 Je\right] \\
&\quad + e_d\left(\frac{Ri_d - P\omega_r L_q i_q - v_d}{L_d}\right) \\
&\quad + e_q\left(\begin{array}{l}\frac{2(B_m - k_1 J)}{3P\psi_m J}\left[T_e - B_m\omega_r - T_L\right] \\ + \frac{Ri_q + P\omega_r L_d i_d + P\omega_r\psi_m - v_q}{L_q}\end{array}\right) \\
&\quad + \frac{1}{\theta_1}\tilde{L}_d\dot{\tilde{L}}_d + \frac{1}{\theta_2}\tilde{L}_q\dot{\tilde{L}}_q + \frac{1}{\theta_3}\tilde{T}_L\dot{\tilde{T}}_L + \frac{1}{\theta_4}\tilde{R}\dot{\tilde{R}}
\end{aligned} \tag{3.15}$$

Now the input voltages v_d and v_q are chosen to make equation 3.15 negative semi definite to ensure global stability.

$$v_d = \hat{R}i_d - P\omega_r\hat{L}_q i_q + k_2 e_d\hat{L}_d + \frac{3P}{2J}\hat{L}_d\left(\hat{L}_d - \hat{L}_q\right)i_q e \tag{3.16}$$

$$\begin{aligned}
v_q = &\frac{2\hat{L}_q(B_m - k_1 J)}{3P\psi_m J}\left[\frac{3P}{2}\left(\psi_m i_q + (\hat{L}_d - \hat{L}_q)i_d i_q\right) - B_m\omega_r - \hat{T}_L\right] \\
&+ \hat{R}i_q + P\omega_r\hat{L}_d i_d + P\omega_r\psi_m + k_3 e_q\hat{L}_q + \frac{3P}{2J}\psi_m e\hat{L}_q
\end{aligned} \tag{3.17}$$

Now substitute equations (3.16) and (3.17) into (3.15) to get

$$\begin{aligned}\dot{V}_1 = &\frac{e}{J}\left[-\tilde{T}_L + \frac{3P}{2}\psi_m e_q + \frac{3P}{2}\left(L_d - L_q\right)e_d i_q - k_1 J e\right] \\ &+\frac{e_d}{\hat{L}_d}\left((R-\hat{R})i_d - P\omega_r(\hat{L}_q - L_q)i_q - k_2 e_d L_d - \frac{3P\hat{L}_d}{2J}(\hat{L}_d - \hat{L}_q)i_q e\right) \\ &+\frac{e_q}{\hat{L}_q}\begin{pmatrix}\frac{\hat{L}_q(B_m - k_1 J)}{\psi_m J}(L_d - \hat{L}_d - L_q + \hat{L}_q)i_d i_q \\ -\frac{2\hat{L}_q(B_m - k_1 J)}{3P\psi_m J}(T_L - \hat{T}_L) + P\omega_r(\hat{L}_d - L_d)i_d \\ +(R-\hat{R})i_q - k_3 e_q \hat{L}_q - \frac{3P}{2J}\psi_m e \hat{L}_q\end{pmatrix} \\ &+\frac{1}{\theta_1}\tilde{L}_d\dot{\tilde{L}}_d + \frac{1}{\theta_2}\tilde{L}_q\dot{\tilde{L}}_q + \frac{1}{\theta_3}\tilde{T}_L\dot{\tilde{T}}_L + \frac{1}{\theta_4}\tilde{R}\dot{\tilde{R}}\end{aligned} \tag{3.18}$$

Simplifying (3.18) we get

$$\begin{aligned}\dot{V}_1 = &-k_1 e^2 - k_2 e_d^2 - k_3 e_q^2 \\ &+\tilde{T}_L\left(\frac{e}{J} + \frac{2e_q(B_m - k_1 J)}{3P\psi_m J} + \frac{1}{\theta_3}\dot{\tilde{T}}_L\right) \\ &+\tilde{L}_d\left(-\frac{3Pee_d i_q}{2J} - \frac{e_q P\omega_r i_d}{L_q} - \frac{e_q(B_m - k_1 J)i_d i_q}{\psi_m J} + \frac{1}{\theta_1}\dot{\hat{L}}_d\right) \\ &+\tilde{L}_q\left(\frac{3Pee_d i_q}{2J} + \frac{e_d P\omega_r i_d}{L_q} + \frac{e_q(B_m - k_1 J)i_d i_q}{\psi_m J} + \frac{1}{\theta_2}\dot{\hat{L}}_q\right) \\ &+\tilde{R}\left(-\frac{e_d i_d}{L_d} - \frac{e_q i_q}{L_q} + \frac{1}{\theta_4}\dot{\hat{R}}\right)\end{aligned} \tag{3.19}$$

From (3.19) we can see the update laws for parameter estimation are

$$\dot{\hat{T}}_L = -\theta_3\left(\frac{e}{J} + \frac{2e_q(B_m - k_1 J)}{3P\psi_m J}\right) \tag{3.20}$$

$$\dot{\hat{L}}_d = \theta_1\left(\frac{3Pee_d i_q}{2J} + \frac{e_q P\omega_r i_d}{L_q} + \frac{e_q(B_m - k_1 J)i_d i_q}{\psi_m J}\right) \tag{3.21}$$

$$\dot{\hat{L}}_q = -\theta_2\left(\frac{3Pee_d i_q}{2J} + \frac{e_d P\omega_r i_d}{L_q} + \frac{e_q(B_m - k_1 J)i_d i_q}{\psi_m J}\right) \tag{3.22}$$

$$\dot{\hat{R}} = \theta_4\left(\frac{e_d i_d}{L_d} - \frac{e_q i_q}{L_q}\right) \tag{3.23}$$

Therefore, the following expression is obtained:

$$\dot{V}_1 = -k_1 e^2 - k_2 e_d^2 - k_3 e_q^2 \tag{3.24}$$

If $k_1, k_2, k_3 > 0$ then it is proved that equation (3.24) guarantees asymptotic stability in the complete system.

3.2 Position Control

For position control, we regard the rotor speed and d-q axis currents as the virtual control variables. The procedure for designing this controller is the same as the previous procedure for speed control. However, in this case the model equations are simplified by grouping parameters into one variable [44]. For convenience, the model is represented as follows.

$$\dot{i}_q = \Phi_1 + a v_q \tag{3.25}$$

$$\dot{i}_d = \Phi_2 + b v_d \tag{3.26}$$

$$T_e = K_T i_q + K_S i_d i_q \tag{3.27}$$

$$\dot{\omega}_r = A i_q + B i_d i_q + C + D\omega_r \tag{3.28}$$

where

$$a = \frac{1}{L_q},\ b = \frac{1}{L_d},\ K_T = \frac{3P}{2}\psi_m\ K_S = \frac{3P}{2}(L_d - L_q)$$

$$A = \frac{K_T}{J},\ B = \frac{K_s}{J},\ C = \frac{-T_L}{J},\ D = \frac{-B_m}{J}$$

and Φ_1 and Φ_2 are defined in Appendix A.2.

Step 1: Define the position tracking error as

$$e_1 = \theta^* - \theta \tag{3.29}$$

where θ^* is the desired reference trajectory of the rotor angle. The position error dynamics is then

$$\dot{e}_1 = \dot{\theta}^* - \dot{\theta} = \dot{\theta}^* - \omega_r \tag{3.30}$$

The stabilizing function is determined by differentiating the Lyapunov function $V_1 = \frac{1}{2}e_1^2$ to get

$$\dot{V}_1 = e_1\dot{e}_1 = e_1(\dot{\theta}^* - \omega_r) \tag{3.31}$$

We now choose the first stabilizing function as

$$\omega_r^* = k_1 e_1 + \dot{\theta}^* \tag{3.32}$$

Equation (3.32) indicates the desired velocity for position tracking. The next step is to design a speed controller so that the rotor speed will follow (3.32).

Step 2: Now we define the speed tracking error as

$$e_2 = \omega_r^* - \omega_r = k_1 e_1 + \dot{\theta}^* - \omega_r \tag{3.33}$$

From equation (3.33), the position error dynamics can be written as

$$\dot{e}_1 = -k_1 e_1 + e_2 \tag{3.34}$$

The speed error dynamics is defined as

$$\dot{e}_2 = \dot{\omega}_r^* - \dot{\omega}_r = -k_1^2 e_1 + k_1 e_2 + \ddot{\theta}^* - A i_q - B i_d i_q - C - D\omega_r \tag{3.35}$$

Now define a new Lyapunov function as

$$V_2 = \frac{1}{2}e_1^2 + \frac{1}{2}e_2^2 \tag{3.36}$$

Differentiate to get

$$\begin{aligned} \dot{V}_2 &= e_1\dot{e}_1 + e_2\dot{e}_2 \\ &= -k_1 e_1^2 + e_2[(1-k_1^2)e_1 + k_1 e_2 \\ &\quad + \ddot{\theta}^* - A i_q - B i_d i_q - C - D\omega_r] \end{aligned} \tag{3.37}$$

Since i_d and i_q were identified as the virtual control variables, we define the reference currents as

$$i_q^* = \frac{1}{A}[(1-k_1^2)e_1 + (k_1+k_2)e_2 + \ddot{\theta}^* - C - D\omega_r] \tag{3.38}$$

$$i_d^* = 0 \tag{3.39}$$

Substituting (3.38) and (3.39) back into equation (3.37) would yield

$$\dot{V}_2 = -k_1 e_1^2 - k_2 e_2^2 \tag{3.40}$$

where $k_1, k_2 > 0$ are design constants. Thus the virtual control is asymptotically stable. Since the parameters C and D are unknown we must use their

estimated values $\hat{C}$ and $\hat{D}$. Thus equation (3.38) becomes

$$\hat{i}_q^* = \frac{1}{A}[(1-k_1^2)e_1 + (k_1+k_2)e_2 + \ddot{\theta}^* - \hat{C} - \hat{D}\omega_r] \tag{3.41}$$

Step 3: The goal now is to make i_d and $\hat{i}_q$ follow the reference trajectory i_d^* and i_q^*. The final current error signals are defined as

$$e_3 = \hat{i}_q^* - i_q \tag{3.42}$$

$$e_4 = i_d^* - i_d \tag{3.43}$$

Using equations (3.42) and (3.43) the speed error dynamics can be represented by

$$\dot{e}_2 = -e_1 - k_2 e_2 + Ae_3 + Be_4 i_q + \tilde{C} + \tilde{D}\omega_r \tag{3.44}$$

where $\tilde{C} = \hat{C} - C$, and $\tilde{D} = \hat{D} - D$ are the parameter estimation errors. Now we define the current error dynamics as

$$\begin{aligned}\dot{e}_3 &= \dot{\hat{i}}_q^* - \dot{i}_q \\ &= \Phi_4 + A\Phi_5 + \tilde{C}\Phi_6 + \tilde{D}\omega_r\Phi_6 + Be_4 i_q(\Phi_6 + \hat{D}\hat{A}^{-1}) - av_q\end{aligned} \tag{3.45}$$

and

$$\dot{e}_4 = -\dot{i}_d = -\Phi_2 - bv_d \tag{3.46}$$

where Φ_4, Φ_5 and Φ_6 are known signals defined in Appendix A.

Step 4: The final Lyapunov function includes the current errors and parameter

estimation errors.

$$V_3 = \frac{1}{2}\left(e_1^2 + e_2^2 + e_3^2 + e_4^2 + \frac{1}{n_1}\tilde{C}^2 + \frac{1}{n_2}\tilde{D}^2\right) \tag{3.47}$$

where n_1, n_2, n_3 are adaptive gains. Now differentiate and substitute all error dynamic equations to get

$$\begin{aligned}
\dot{V}_3 &= e_1\dot{e}_1 + e_2\dot{e}_2 + e_3\dot{e}_3 + e_4\dot{e}_4 + \frac{1}{n_1}\tilde{C}\dot{\tilde{C}} + \frac{1}{n_2}\tilde{D}\dot{\tilde{D}} \qquad (3.48)\\
&= e_1(-k_1e_1 + e_2) + e_2(-e_1 - k_2e_2 + Ae_3 + Be_4i_q \\
&\quad +\tilde{C} + \tilde{D}\omega_r) + e_3(\Phi_4 + A\Phi_5 + \tilde{C}\Phi_6 + \tilde{D}\omega_r\Phi_6 - av_q) \\
&\quad +e_4(-\Phi_2 - bv_d) + \frac{1}{n_1}\tilde{C}\dot{\tilde{C}} + \frac{1}{n_2}\tilde{D}\dot{\tilde{D}} \\
&= -k_1e_1^2 - k_2e_2^2 - k_3e_3^2 - k_4e_4^2 + Ae_2e_3 \\
&\quad +\tilde{C}(e_2 + \Phi_6e_3 + \frac{1}{n_1}\dot{\tilde{C}}) \\
&\quad +\tilde{D}(e_2\omega_r + \Phi_6e_3\omega_r + \frac{1}{n_2}\dot{\tilde{D}}) + e_3(k_3e_3 + \Phi_4 - av_q) \\
&\quad +e_4(k_4e_4 + Bi_q(e_2 + \Phi_6 + \hat{D}A^{-1}) - \Phi_2 - bv_q) \qquad (3.49)
\end{aligned}$$

The d-q axis reference voltages are chosen to be

$$v_q^* = \frac{1}{a}(k_3e_3 + \Phi_4) \tag{3.50}$$

$$v_d^* = \frac{1}{b}(k_4e_4 + Bi_q(e_2 + \Phi_6 + \hat{D}A^{-1}) - \Phi_2) \tag{3.51}$$

where $k_3, k_4 > 0$ are design constants. The update laws are defined as

$$\dot{\hat{C}} = -n_2(e_2 + \Phi_6e_3) \tag{3.52}$$

$$\dot{\hat{D}} = -n_3(e_2\omega_r + \Phi_6e_3\omega_r) \tag{3.53}$$

Substituting equation (3.50-3.53) into equation (3.49) would yield

$$\dot{V}_3 = -k_1 e_1^2 - k_2 e_2^2 - k_3 e_3^2 - k_4 e_4^2 + A e_2 e_3 < 0 \tag{3.54}$$

for sufficiently large k_2 and k_3. Thus it is shown that the complete system is asymptotically stable.

Chapter 4

Simulation of the Complete IPMSM Drive System

The dynamics of the IPMSM is complex because of its nonlinear nature and also the discrete time nature of the inverter and motor system. Therefore, after developing the control strategy of the complete drive system, digital simulations are performed to predict the behaviour of the system before it is implemented in real time. The simulation of the proposed drive system has been carried out using MATLAB/Simulink software [45]. In order to simulate the motor model in Simulink, the state space equations (2.25)-(2.27) describing the IPMSM are used.

4.1 Speed Control

In order to verify the effectiveness of the proposed adaptive scheme, digital simulations have been performed using Matlab/Simulink software. The overall objective in a high performance drive application is to force the output speed of the motor to follow a desired speed trajectory with little or no error.

4.1.1 Drive System

Based on the control principle described in Section 3.1 the complete closed loop vector control scheme of the IPMSM is shown in Figure 4.2. The details of each subsystem are given in Appendix B. First, the command current i_q^* and the estimated load torque are calculated online based on speed error and the actual d-q axis currents i_d and i_q using equations (3.13) and (3.20) respectively. From these values, the parameters R, L_d and L_q are estimated using equations (3.21) to (3.23). Finally, the control voltages v_d and v_q are calculated using equations (3.16) and (3.17). Then, they are converted to 3-phase voltages using Park's transformation [10]. The PWM signals are generated by comparing the 3-phase voltages with high frequency triangular waveforms as shown in Figure 4.3 The phase voltages are expressed as a function of bus voltage V_B and logic variables NA,NB and NC as

$$\begin{bmatrix} v_a \\ v_b \\ v_c \end{bmatrix} = \frac{1}{3} \begin{bmatrix} 2 & -1 & -1 \\ -1 & 2 & -1 \\ -1 & -1 & 2 \end{bmatrix} \begin{bmatrix} NA \\ NB \\ NC \end{bmatrix} V_B \tag{4.1}$$

where v_{abc} are the phase voltages. The PWM logic signals operate the inverter switches which run the motor. The three phase currents i_{abc} are converted to d-q axis currents which is fed back into the controller along with the speed which completes the closed loop system.

4.1.2 Simulation Results and Discussion

For a sample comparison, a conventional PI controller was designed and simulated, and the results are shown. The block diagram Proportional gain K_P and integral gain K_I were chosen to be 0.6 and 0.07 respectively by trial and

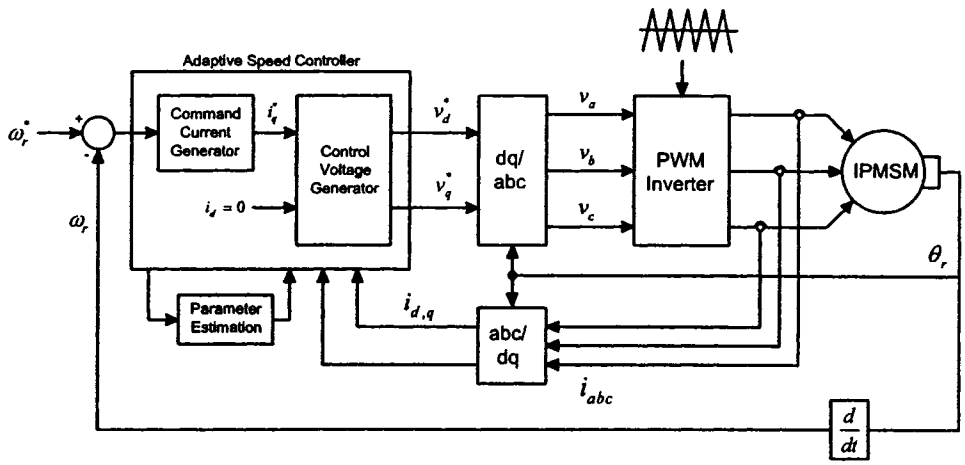

Figure 4.1: Block diagram for adaptive backstepping based speed control of the proposed drive

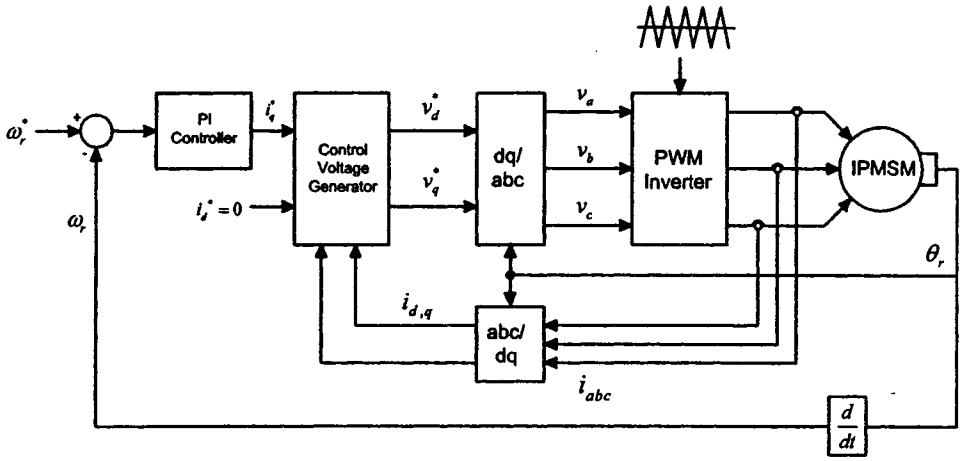

Figure 4.2: Block diagram for PI speed control of the proposed drive

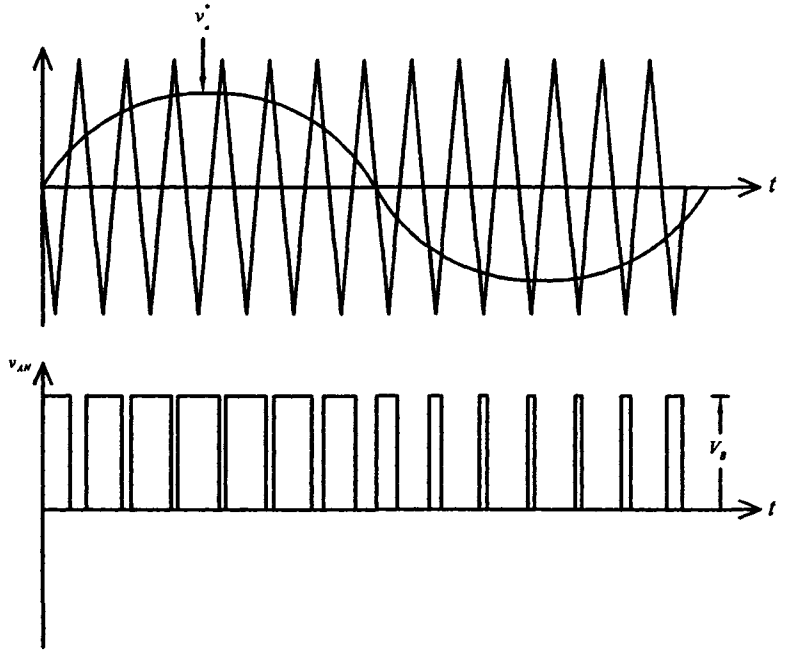

Figure 4.3: PWM signal generation by comparing high frequency triangular waveform with command voltage

error in order to maintain minimum settling time, overshoot and zero steady state error. Figure 4.4 shows the response of the IPMSM drive with a PI controller at rated speed and no load conditions. The speed response has a large over shoot and settling time. However, the drive follows the command speed with little steady state error.

Figure 4.5(a) shows the speed response of the proposed adaptive backstepping based nonlinear (ABNL) controller and drive system from a step change in reference speed from 0 rad/sec to 188.5 rad/sec (1800 rpm) at no load ($T_L = 0Nm$). The actual speed converges with the reference speed in a very short time with minimal overshoot and no steady state error. Figure 4.5(b) shows the corresponding d-q axis motor currents along with the command q-axis current and figure 4.5(c) shows the actual motor current i_a. The output voltage from the PWM inverter is shown in Fig. 4.5(d). Figures 4.6(a) to 4.6(c) show the corresponding speed and current errors which all converge to zero. This was the goal in designing the controller. The overall stability of the system is shown by a plot of i_{ds} vs i_{qs} in Figure 4.6(d).

Figure 4.7(a) shows the speed response for a step change in reference speed at full load $T_L = 2Nm$). Again, the actual speed converges with the reference speed with no steady state error. The motor currents are shown in Figs 4.7(b) and 4.7(c). Figure 4.7(d) shows the estimated and actual values of load torque. Next the same results are shown for the motor at low speed (0 to 50 rad/sec). The speed response takes a bit longer to converge to the reference speed as shown in Fig.4.8(a), but there is still no overshoot and no steady state error. The motor currents and voltage in Figs.4.8(b) to 4.8(d) show no difference than the previous results.

Figure 4.9 shows the response of the IPMSM drive with a PI controller

with a step change in load from $0Nm$ to $1Nm$ at 1.2 seconds. When the load disturbance is introduced there is a noticeable drop in speed which takes time to recover. The corresponding motor currents are shown in Fig. 4.9(b) and 4.9(c) and the steady state *abc* currents are shown in Fig. 4.9(d). Next the results are shown in Fig. 4.9 for a sudden change in load torque from $1Nm$ to $2Nm$ at rated speed for the proposed controller. The disturbance was applied at 1.5 seconds. As can be shown in Fig.4.10(a) there is very little change in speed when the load was applied, and the speed recovered in a very short time. This shows the superiority of the proposed controller over the PI controller. Figures 4.10(b) and 4.10(c) show the corresponding motor current i_a and Fig. 4.10(d) shows the steady state i_{abc} currents. Next, the corresponding estimated parameters are shown in Fig. 4.11, which are the load torque, stator resistance and d-q axis inductances L_d and L_q. Next the results are shown for step change in parameters R and L_q in Figure 4.12. It is evident that the proposed controller can handle the parameter variations without any deviation in speed. No noticeable variation in speed is present; therefore the controller is insensitive to parameter variations.

Figure 4.13 shows the results for step change in load but with no adaptation of load torque in the controller. This is to demonstrate the need for parameter adaptation. As can be shown in Fig. 4.13(a) the speed does not converge back to the command speed when the load disturbance is introduced. Since the parameter is fixed in the controller, any deviation of actual load torque will produce an error in speed. Figs.4.13(b) to 4.13(d) show the corresponding speed error and d-q axis current errors respectively.

Next, the results are shown for a sudden step change in command speed. As shown in Figure 4.14(a), the initial command speed is set to 100 rad/sec

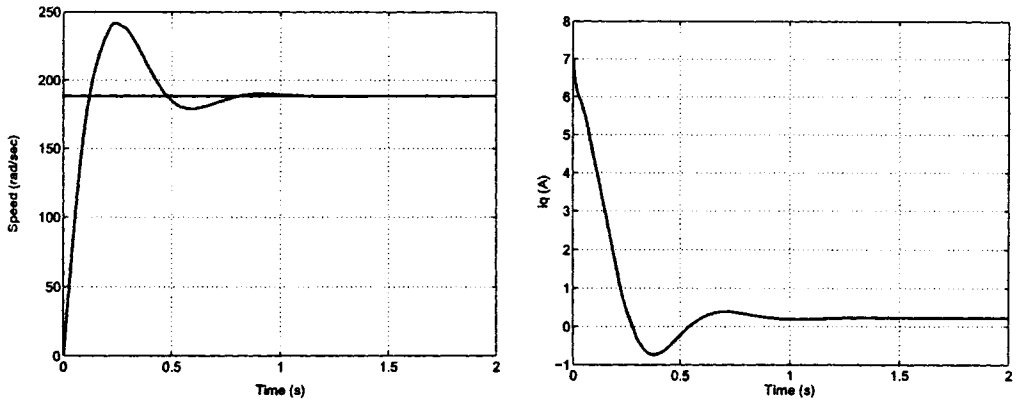

(a) Speed response

(b) q-axis motor current i_q

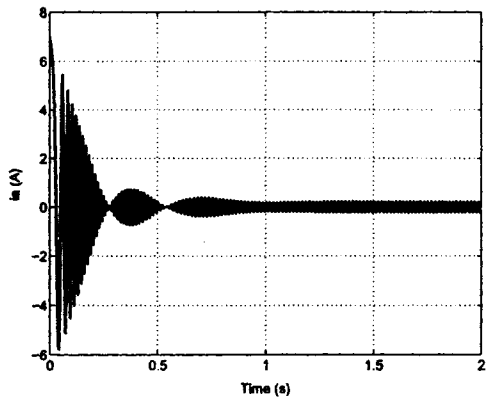

(c) Motor current i_a

Figure 4.4: Simulated response of the drive under PI control at rated speed (188.5 rad/sec) and no load conditions.

and is changed to 188.5 rad/sec at $t = 1$ second and then down to 40 rad/sec at $t = 2$ seconds. Figure 4.14(b) to 4.14(d) show the corresponding d-q axis currents and load torque estimation respectively. These results also validate the robustness of controller. Figure 4.15 shows the results for a reverse change in command speed at full load conditions. These results are similar to the previous results for step change in command speed.

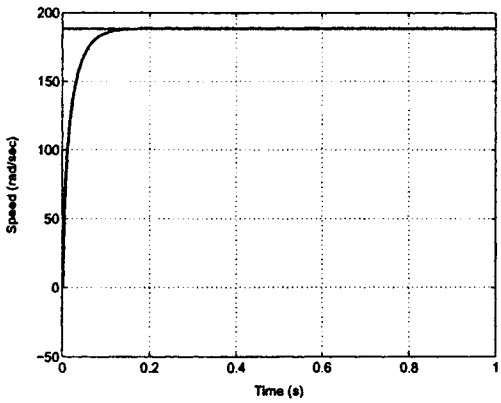

(a) Speed response

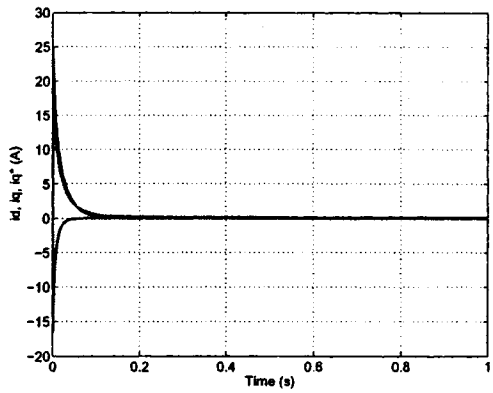

(b) Command q-axis current and d-q axis motor currents i_q^*, i_q, i_d

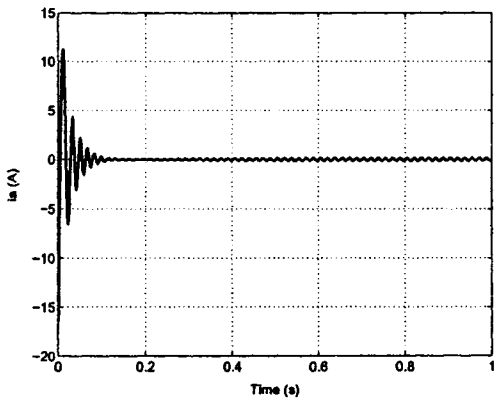

(c) Motor current i_a

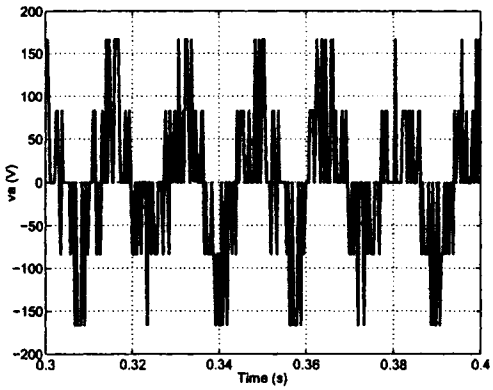

(d) Output voltage from PWM inverter

Figure 4.5: Simulated responses of the proposed ABNL controller and drive at no load and rated speed (188.5 rad/sec).

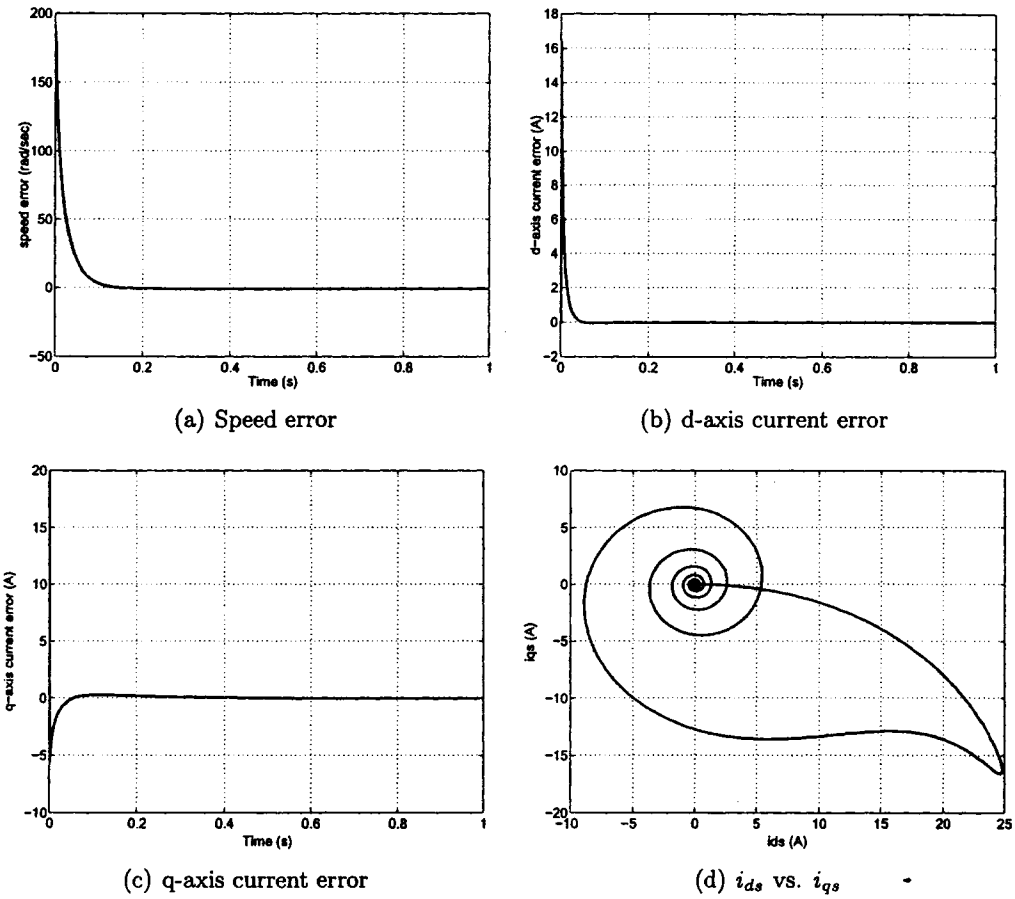

(a) Speed error

(b) d-axis current error

(c) q-axis current error

(d) i_{ds} vs. i_{qs}

Figure 4.6: Simulated responses of the proposed ABNL controller and drive at no load and rated speed (188.5 rad/sec).

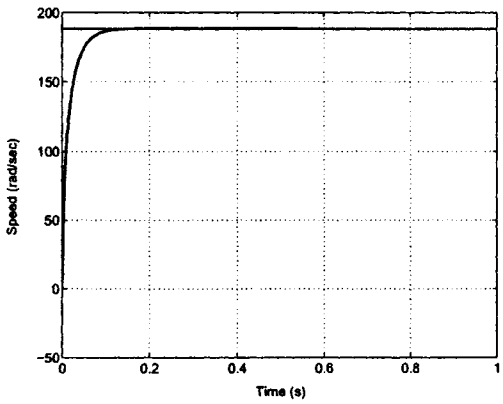

(a) Speed response

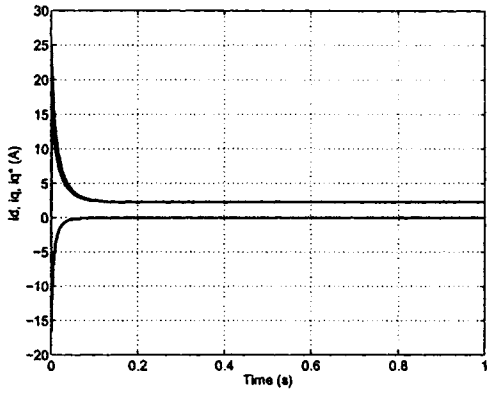

(b) Command q-axis current and d-q axis motor currents i_q^*, i_q, i_d

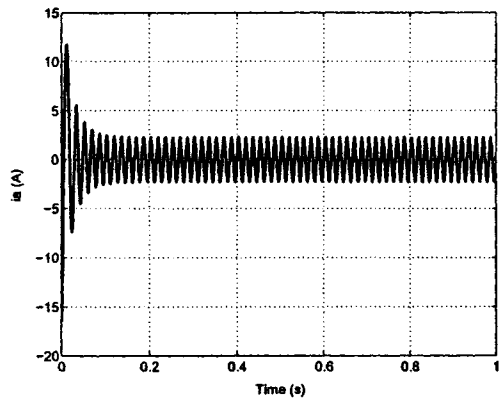

(c) Motor current i_a

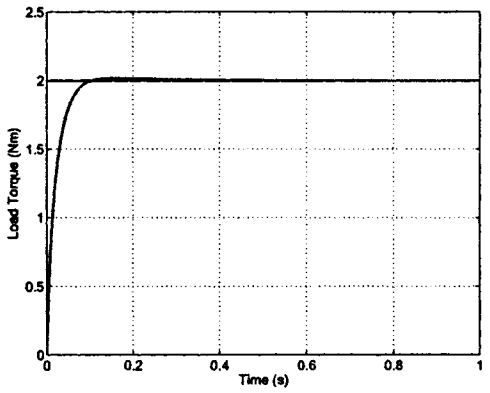

(d) Estimated and actual load torque

Figure 4.7: Simulated responses of the proposed ABNL controller and drive at full load and rated speed (188.5 rad/sec).

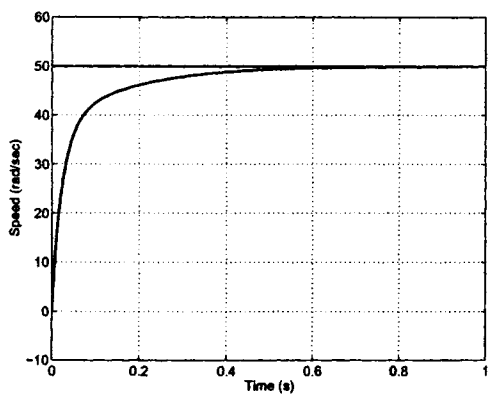

(a) Speed

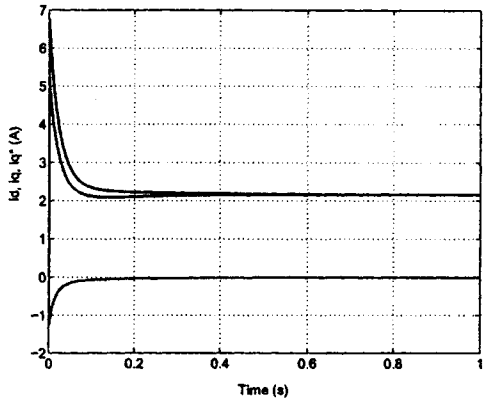

(b) Command q-axis current and d-q axis motor currents i_q^*, i_q, i_d

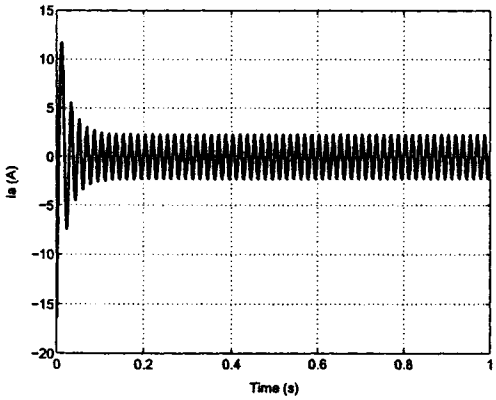

(c) Motor current i_a

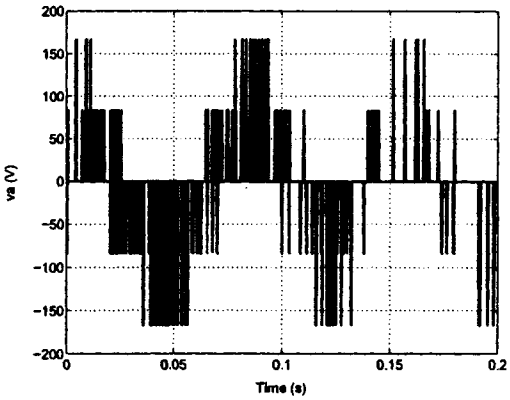

(d) Output voltage from PWM inverter

Figure 4.8: Simulated responses of the proposed ABNL controller and drive at full load and low speed (50 rad/sec).

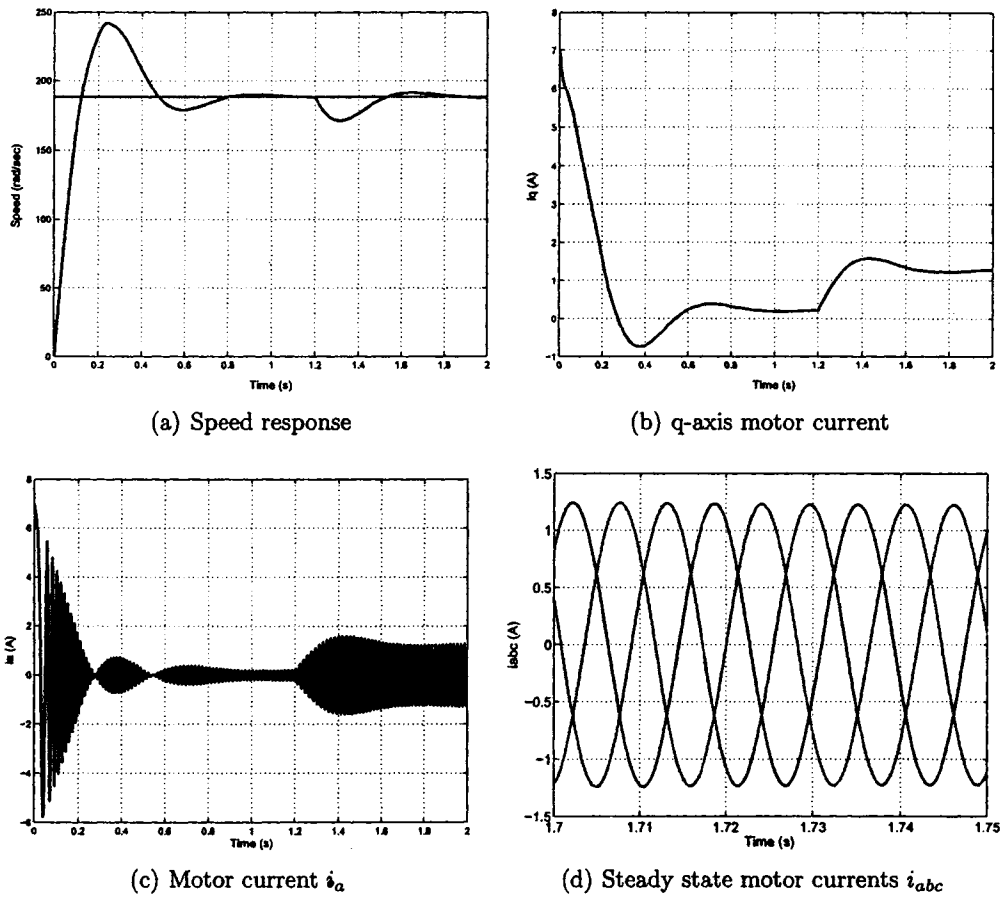

(a) Speed response

(b) q-axis motor current

(c) Motor current i_a

(d) Steady state motor currents i_{abc}

Figure 4.9: Simulated response of the drive under PI control with step change in load.

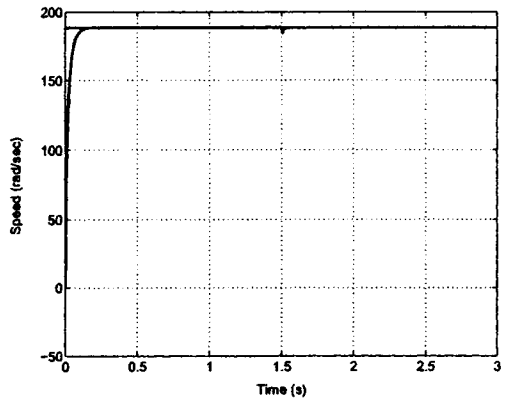

(a) Speed

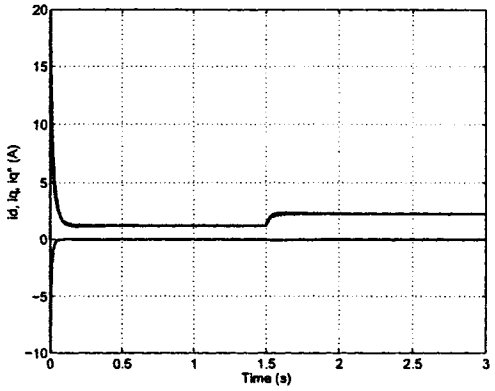

(b) Command q-axis current and d-q axis motor currents i_q^*, i_q, i_d

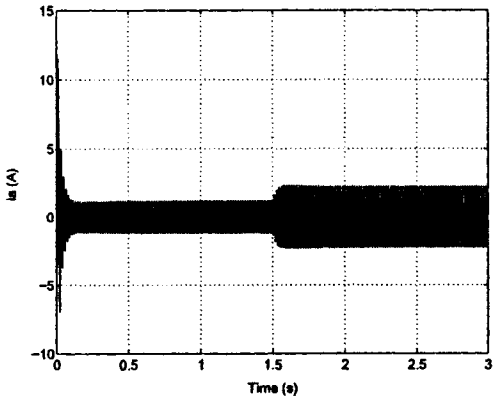

(c) Motor current i_a

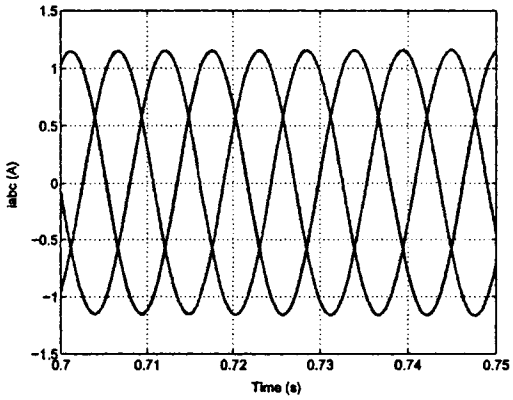

(d) Steady state motor currents i_{abc}

Figure 4.10: Simulated responses of the proposed ABNL controller and drive at rated speed with step change in load torque (1 Nm to 2 Nm).

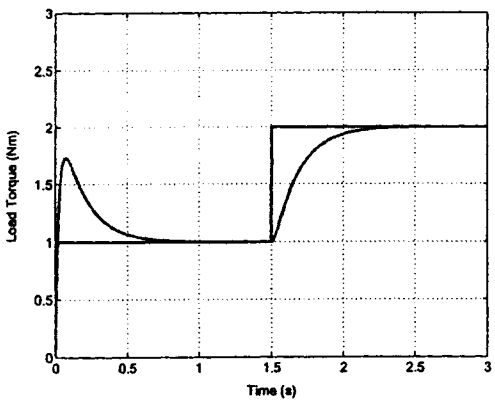

(a) Estimated and actual load torque.

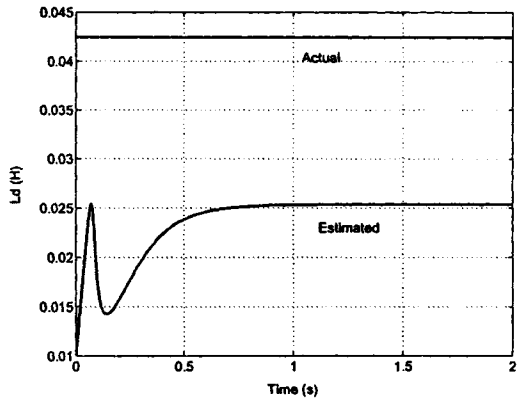

(b) Estimated and actual d-axis inductance L_d

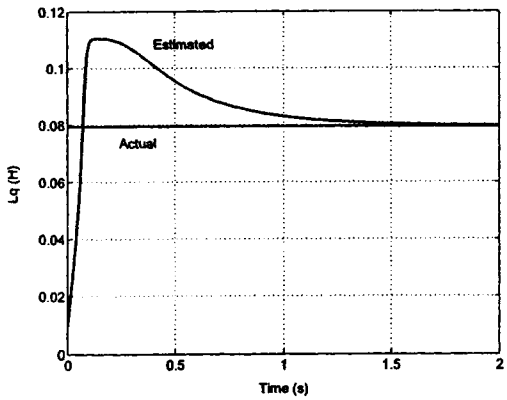

(c) Estimated and actual q-axis inductance L_q

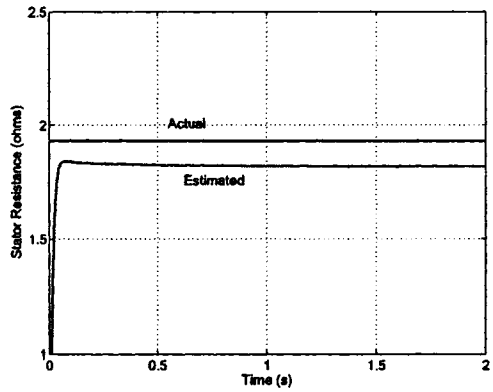

(d) Estimated and actual stator resistance.

Figure 4.11: Simulated responses of the proposed ABNL controller and drive at rated speed with step change in load torque (1 Nm to 2 Nm).

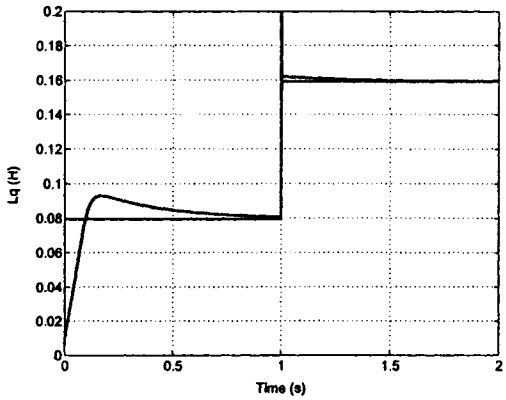

(a) Estimated and actual q-axis inductance L_q.

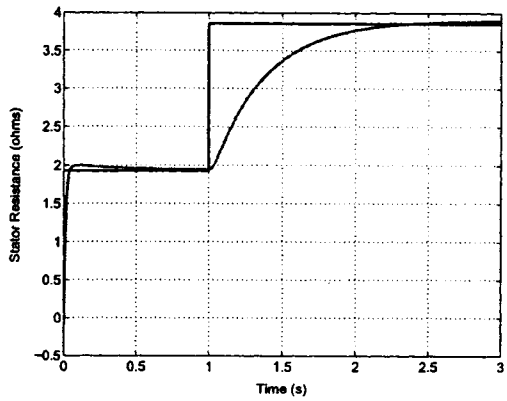

(b) Estimated and actual stator resistance R

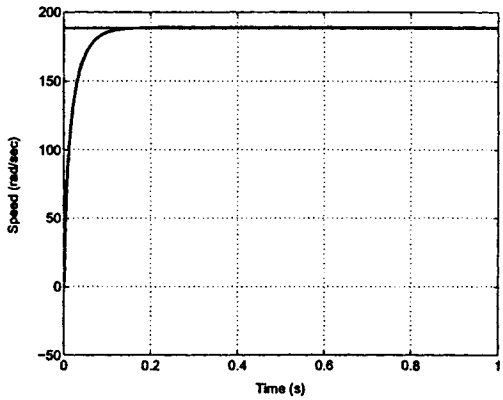

(c) Speed response for both conditions.

Figure 4.12: Simulated responses of the proposed ABNL controller and drive at rated speed with step change in stator resistance and q-axis inductance.

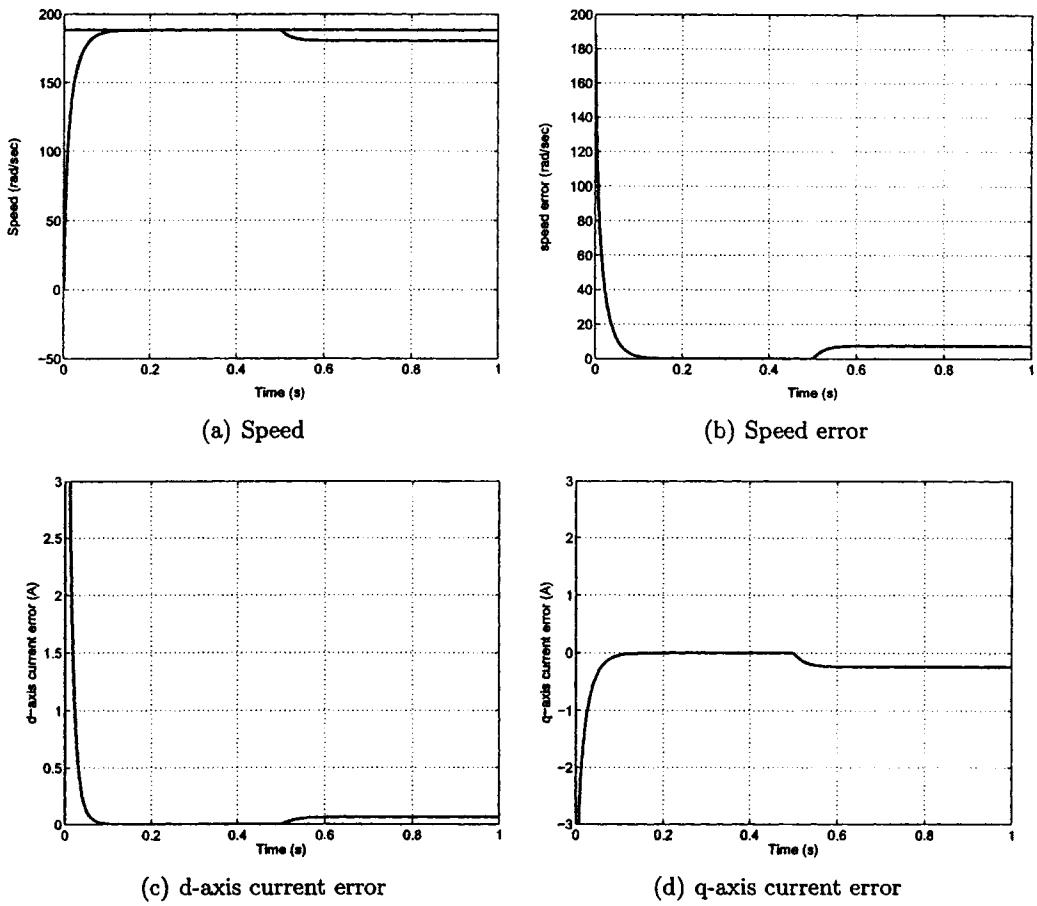

(a) Speed

(b) Speed error

(c) d-axis current error

(d) q-axis current error

Figure 4.13: Simulated responses of the proposed ABNL controller and drive at rated speed with step change in load torque (1 Nm to 2 Nm) with no adaptation in controller.

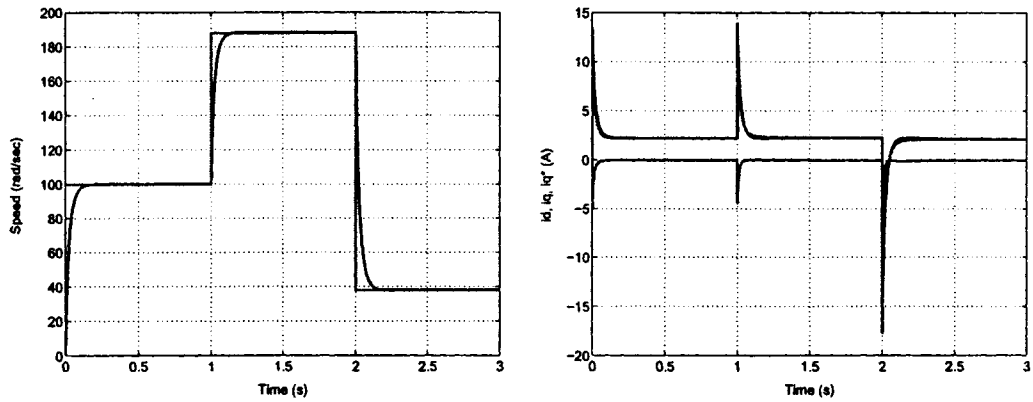

(a) Speed

(b) Command q-axis current and d-q axis motor currents i_q^*, i_q, i_d

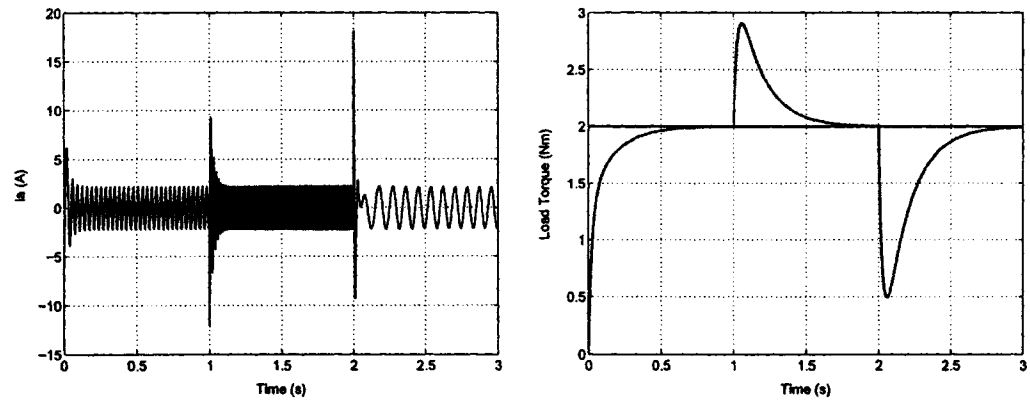

(c) Motor current i_a

(d) Estimated and actual load torque

Figure 4.14: Simulated responses of the proposed ABNL controller and drive at full load with step change in command speed.

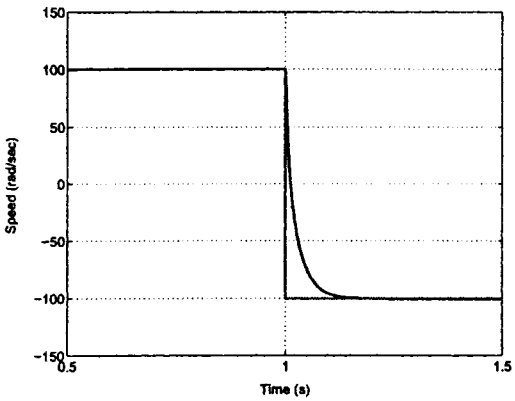

(a) Speed

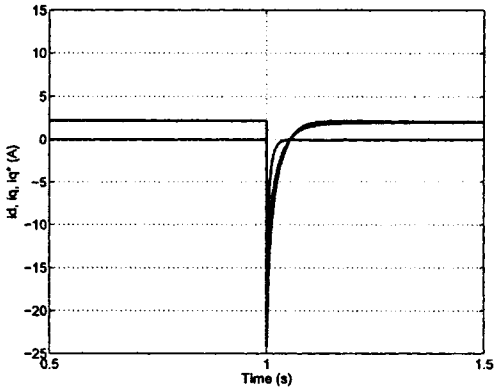

(b) Command q-axis current and d-q axis motor currents i_q^*, i_q, i_d

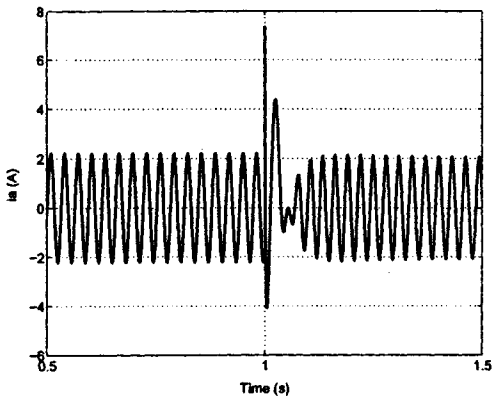

(c) Motor current i_a

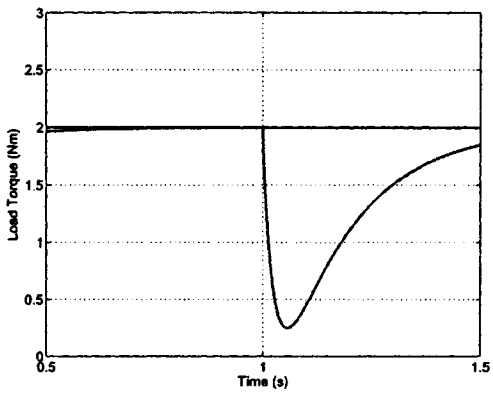

(d) Estimated and actual load torque

Figure 4.15: Simulated responses of the proposed ABNL controller and drive at full load with reverse change in command speed.

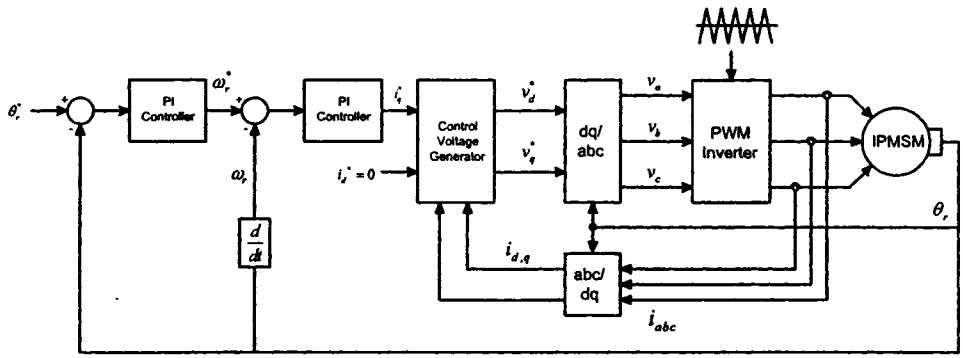

Figure 4.16: Block diagram for PI based position control

4.2 Position Control

4.2.1 Drive System

Based on the control principle in section 3.2 the complete closed loop vector control scheme of the IPMSM is shown in Figure 4.17. First the command speed is calculated from the position error and derivative of the command position using equation (3.32). The speed controller then generates the command d-q axis currents using equations (3.41) and (3.39) respectively. Parameters C and D are calculated using equations (3.52) and (3.53) and the actual d-q axis stator currents. Then the control voltages v_q and v_d are calculated using equations (3.50) and (3.51), respectively. Then they are converted to 3-phase voltages using Park's Transformation. The PWM signals are generated by comparing the 3-phase voltages with high frequency triangular waveforms. The PWM logic signals operate the inverter switches which run the motor.

4.2.2 Simulation Results and Discussion

In order to verify the effectiveness of the proposed adaptive scheme for position control of the IPMSM, digital simulations have been performed using

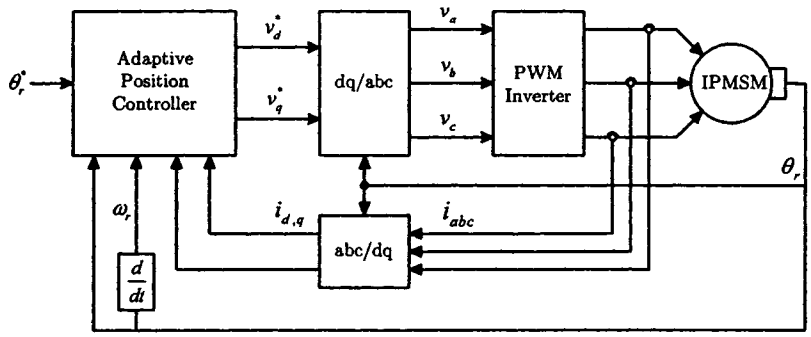

(a) General block diagram

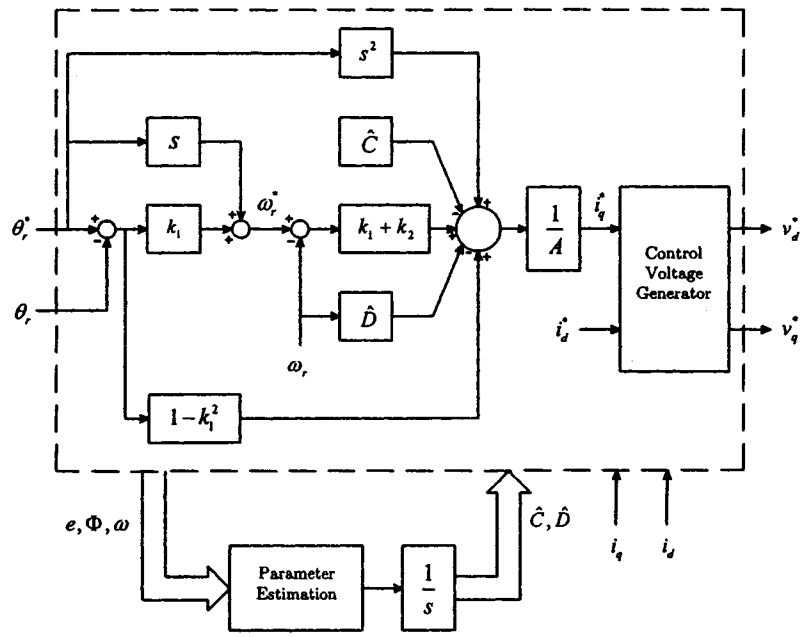

(b) Detailed block diagram of the adaptive position controller

Figure 4.17: Block diagrams for position control

Matlab/Simulink software [45]. The overall control bock diagram is shown in Figure 4.17(a) and a detailed block diagram of the adaptive controller is shown in Figure 4.17(b). Numerous simulations were performed, and some sample results are shown here. Figure 4.18(a) shows the rotor position for a sinusoidal reference trajectory $\theta^* = 90\sin(2t)$. Load torque was set to 2 Nm. The rotor position follows the reference trajectory with little error. Figure 4.18(b) shows the corresponding command speed and actual speed, figure 4.18(c) shows the d-q axis currents and figure 4.18(d) shows the command voltages v_d^* and v_q^*. The motor current i_a, voltage v_a, PWM output voltage and estimated load torque are shown in Figs. 4.19(a) to 4.19(d) respectively. All the controller error values are shown in Figure 4.20. There is some small steady state error in the position, speed and currents.

For comparison, the drive was also simulated under PI control. The block diagram is shown in Figure 4.16 In the outer position control loop, K_P and K_I were 1.2 and 7 respectively. For the inner speed control loop, K_P and K_I were 0.6 and 0.07 respectively. The results are shown in Figure 4.21. The output rotor position does not converge to the command position for sine wave trajectory, and there is a large overshoot and long settling time for square wave trajectory.

Now the results are shown for square wave trajectory. Figure 4.22(a) shows the rotor position for a step change in reference position. The actual position converges to the reference position in a short time with no overshoot and no steady state error. Figure 4.22(b) to 4.22(d) show the corresponding speed, currents and voltages. At 3.5 seconds, the load torque was changed from 1 to 2 Nm. There is no noticeable change in the position results. Figures 4.23(a) to 4.23(d) show all controller error values. In this case all errors converge to

zero which was the goal in designing the controller. Figure 4.24 shows the estimated value of C and D which is the inverse mechanical time constant of the motor for square and sine wave trajectories. The estimated values does not converge to the constant actual value due to the online adaptive nature of the controller.

4.3 Concluding Remarks

An adaptive backstepping based nonlinear control technique for an IPMSM drive has been developed for both position and speed control. The control laws were derived based on the motor model incorporating various system uncertainties. Global stability of the developed nonlinear controller has been verified analytically using Lyapunov's stability theory. As shown by the simulation results, speed tracking and position tracking were achieved with no steady state error or overshoot. The performance of these controllers was found to be superior to the drive under PI control.

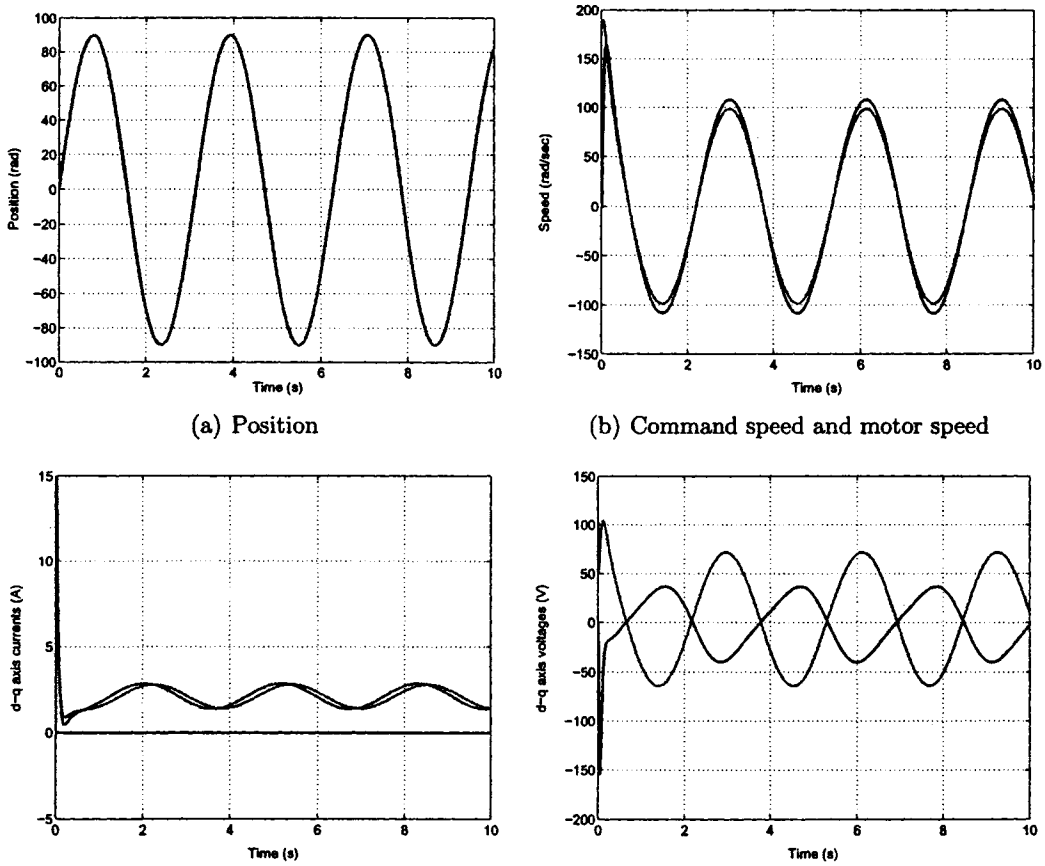

(a) Position

(b) Command speed and motor speed

(c) Command q-axis current and d-q axis motor currents i_q^*, i_q, i_d

(d) Command d-q axis motor voltages v_d^*, v_q^*

Figure 4.18: Simulated responses of the proposed ABNL position controller and drive for sine wave trajectory.

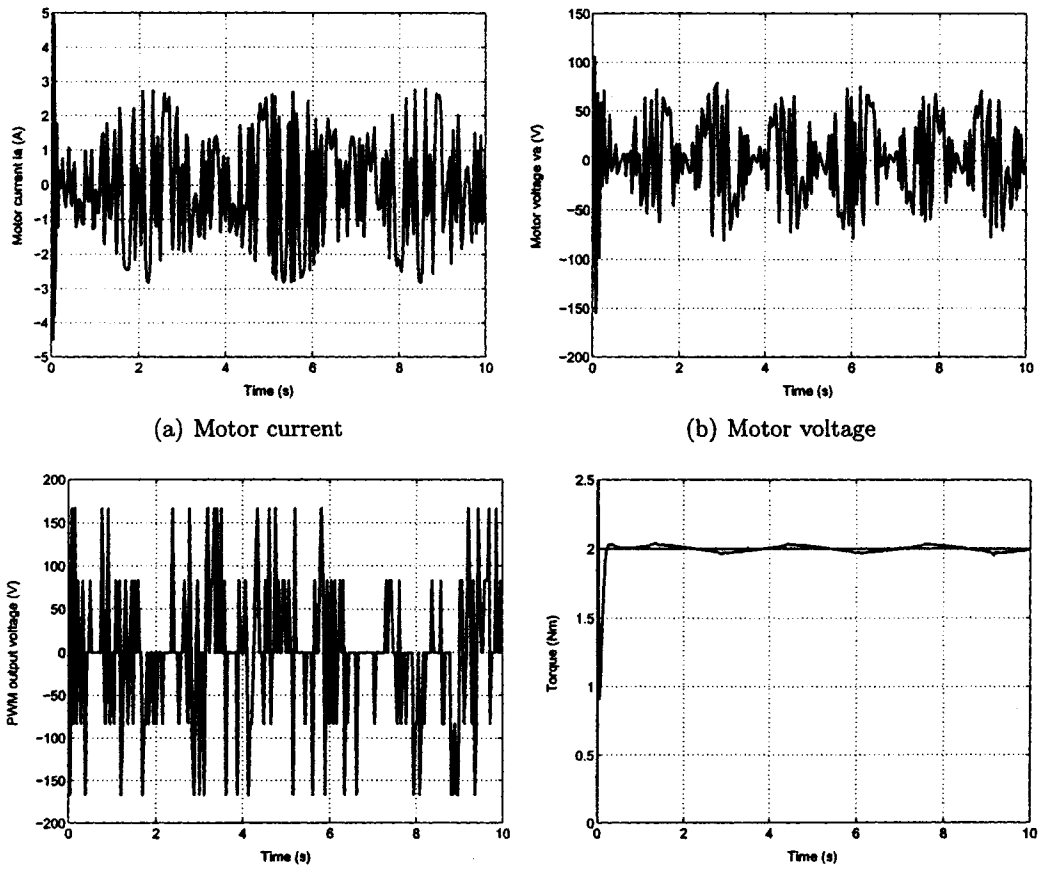

(a) Motor current

(b) Motor voltage

(c) Output voltage of PWM inverter

(d) Estimated and actual load torque

Figure 4.19: Simulated responses of the proposed ABNL position controller and drive for sine wave trajectory.

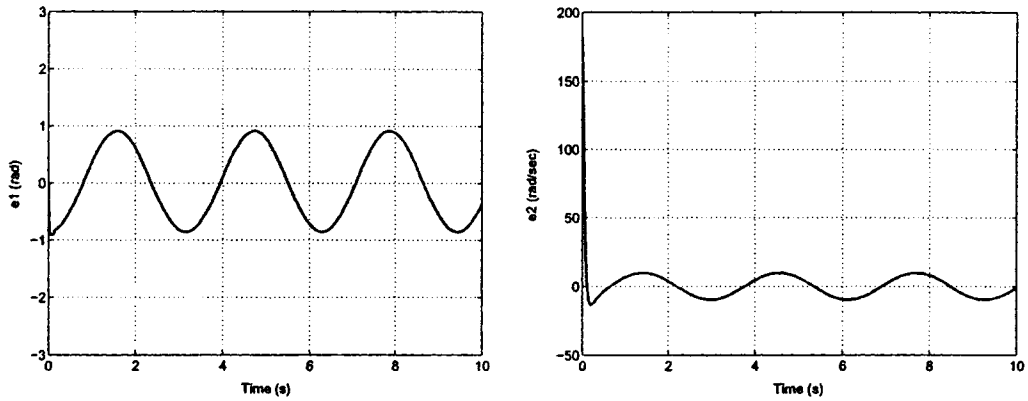

(a) Position error

(b) Speed error

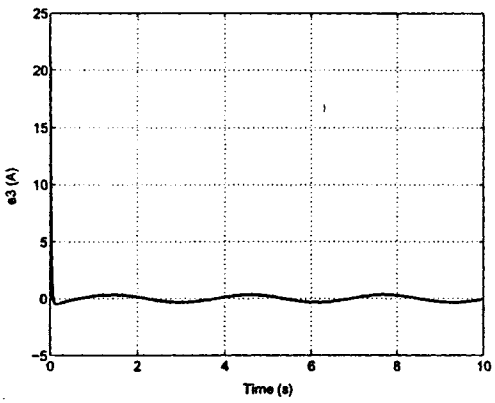

(c) q-axis current error

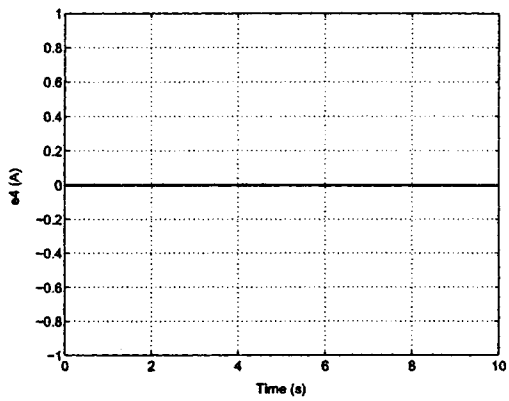

(d) d-axis current error

Figure 4.20: Simulated responses of the proposed ABNL position controller and drive for sine wave trajectory.

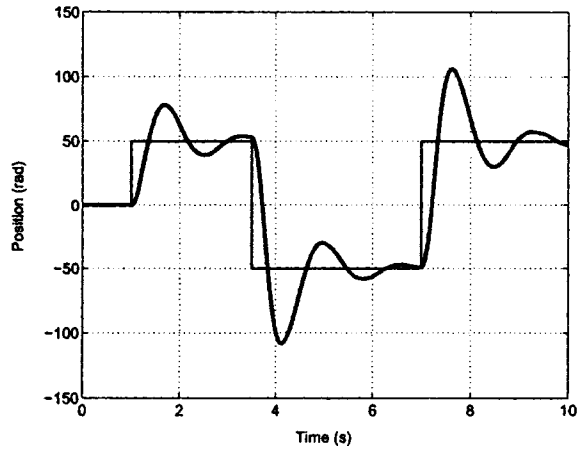

(a) Square wave

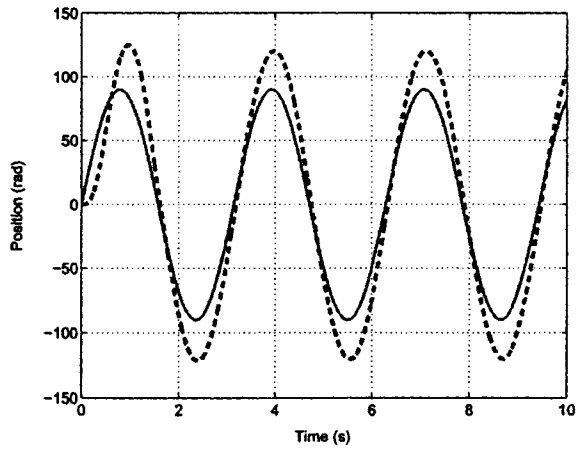

(b) Sine wave

Figure 4.21: Simulated responses of the system under PI control for square and sine wave trajectory. The dotted line represents the rotor position and the solid line represents the command position.

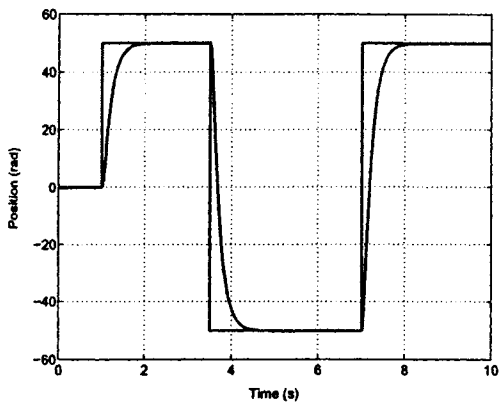

(a) Position

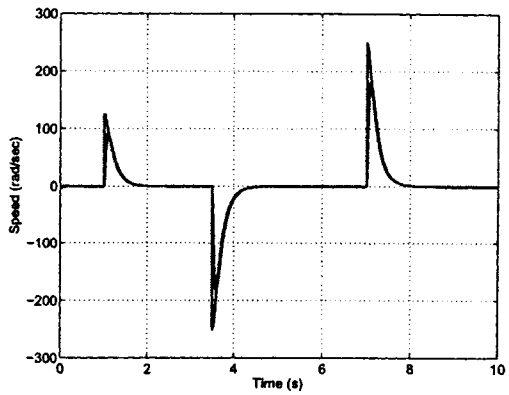

(b) Command speed and motor speed

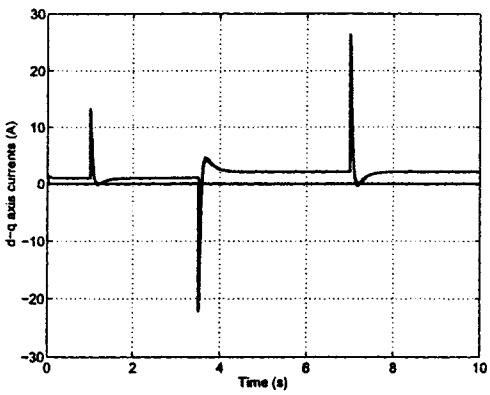

(c) Command q-axis current and d-q axis motor currents i_q^*, i_q, i_d

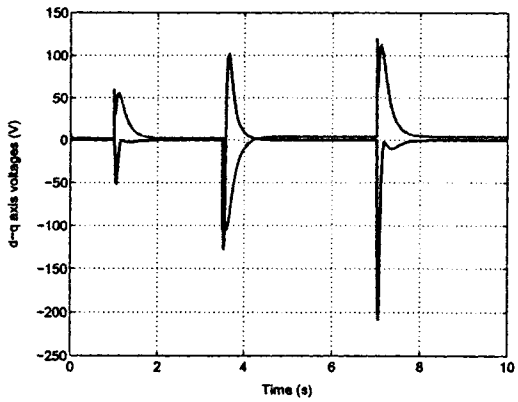

(d) Command d-q axis motor voltages v_d^*, v_q*

Figure 4.22: Simulated responses of the proposed ABNL position controller and drive for square wave trajectory.

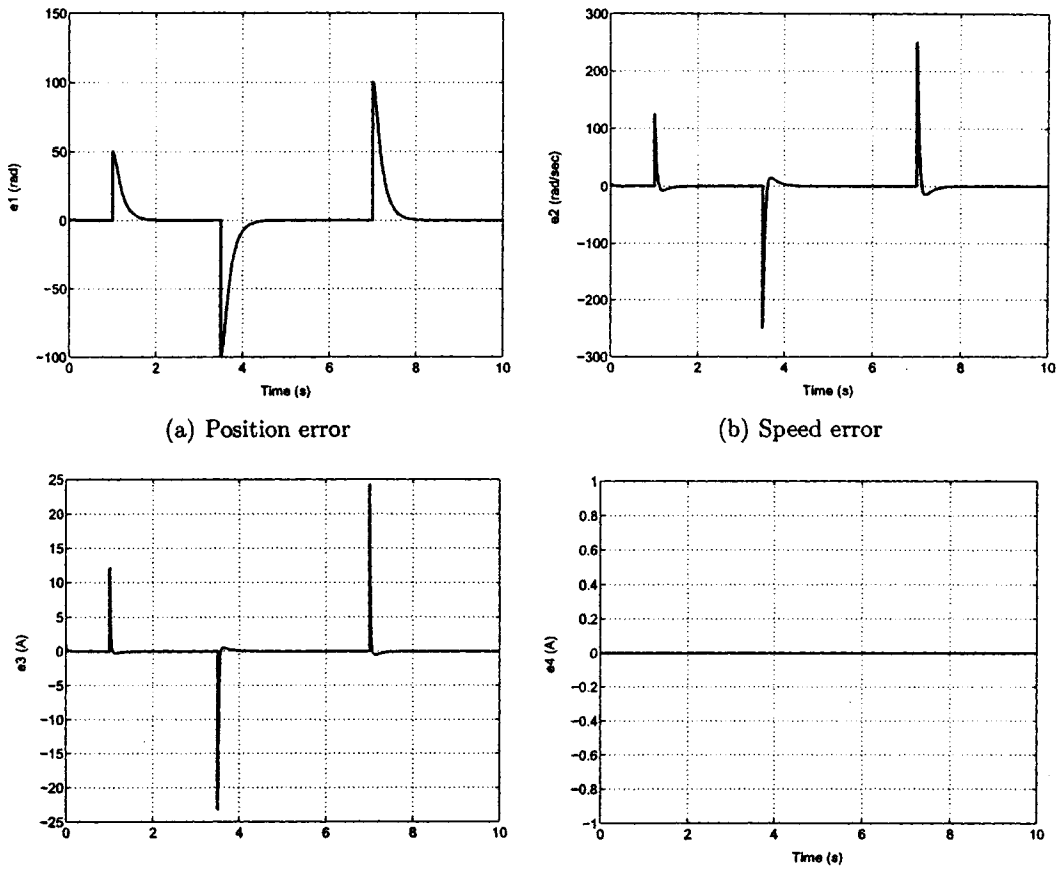

(a) Position error

(b) Speed error

(c) q-axis current error

(d) d-axis current error

Figure 4.23: Simulated responses of the proposed ABNL position controller and drive for sine wave trajectory.

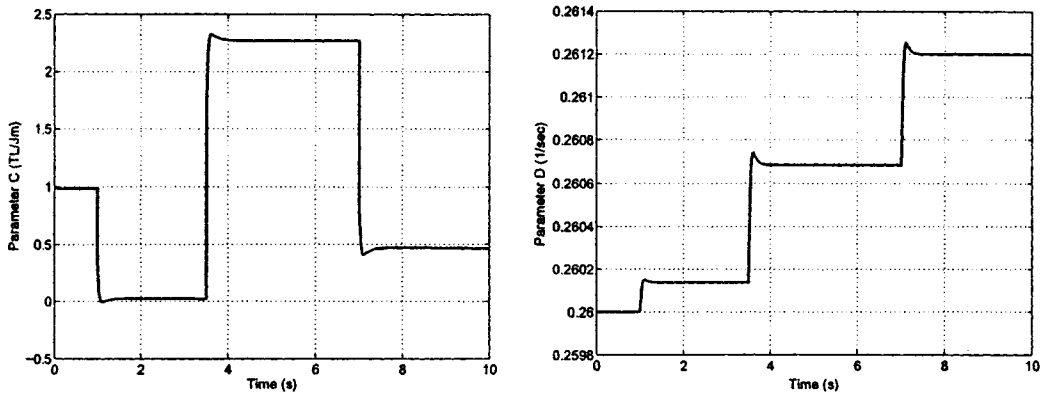

(a) Estimated value of C for square wave

(b) Estimated value of D for square wave

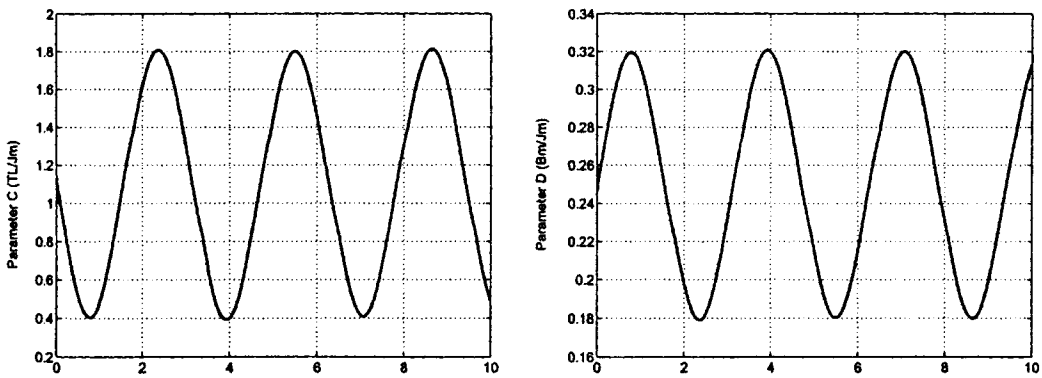

(c) Estimated value of C for sine wave

(d) Estimated value of D for sine wave

Figure 4.24: Simulated parameter estimation responses of the proposed ABNL position controller and drive for sine and square wave trajectories.

Chapter 5

Experimental Implementation

After the performance of the drive was tested in simulation, the results of the proposed drive were found to be satisfactory for an attempt of real time implementation. An attempt was made to implement the complete drive in real time both through hardware and software. Due to time constraints, this section was not completely finished, however, most of the setup has been completed and it is only a matter of integrating the entire system.

5.1 Experimental Setup

In order to implement the control scheme in real time the DSP board DS1104 is used [46]. The board is installed in an Intel PC with uninterrupted communication through dual port memory. The DS1104 board is mainly based on a Texas Instrument MPC8240 64-bit floating point digital signal processor. The DSP is supplemented by a set of on-board peripherals used in digital control systems including analog to digital (A/D), digital to analog (D/A) converters and incremental encoder interfaces. Also, it is equipped with a TI TMS320F240 16-bit micro controller DSP that acts as a slave processor and

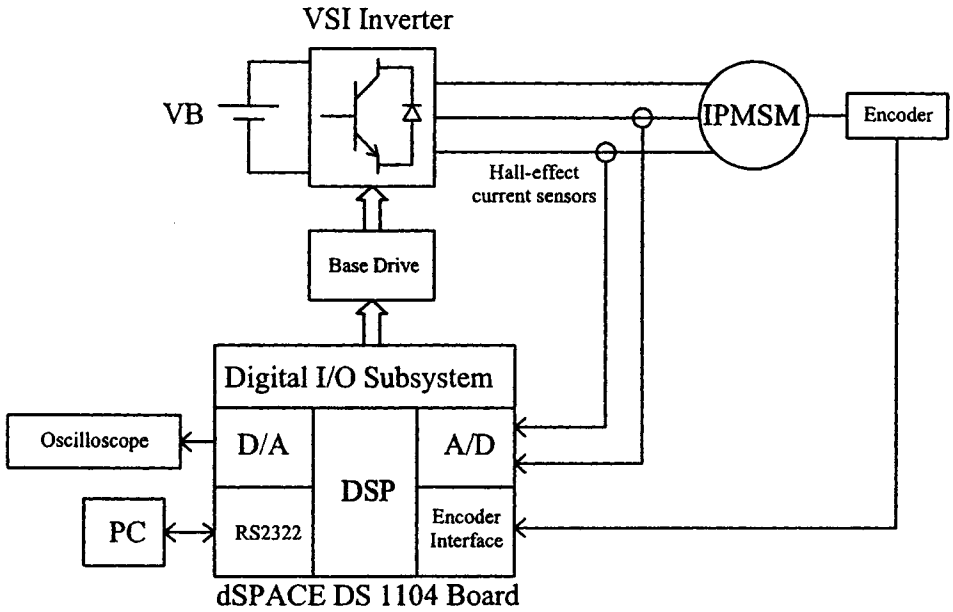

Figure 5.1: Block diagram of the hardware schematic of the VSI-fed IPMSM drive

provides the necessary digital I/O ports and powerful timer functions such as input capture, output capture and PWM generation. The block diagram of the hardware schematic is shown in Figure 5.1. The actual motor currents are measured by the Hall-effect sensors and then fed back to the DSP board through the A/D channel. Rotor position is sensed by an optical incremental encoder mounted at the rotor shaft and is fed back to the DSP board through the encoder interface. The outputs of the DSP board are six PWM signals that are sent directly to the base drive circuit of the inverter.

In order to implement the control algorithm, a real-time Simulink model for the complete drive system is developed which is shown in Figure B.7. Then the model is downloaded to the DSP board using the Control Desk software. The high level C code is generated from the Simulink model.

The flow chart of the software is shown in Figure 5.2. The timer interrupt

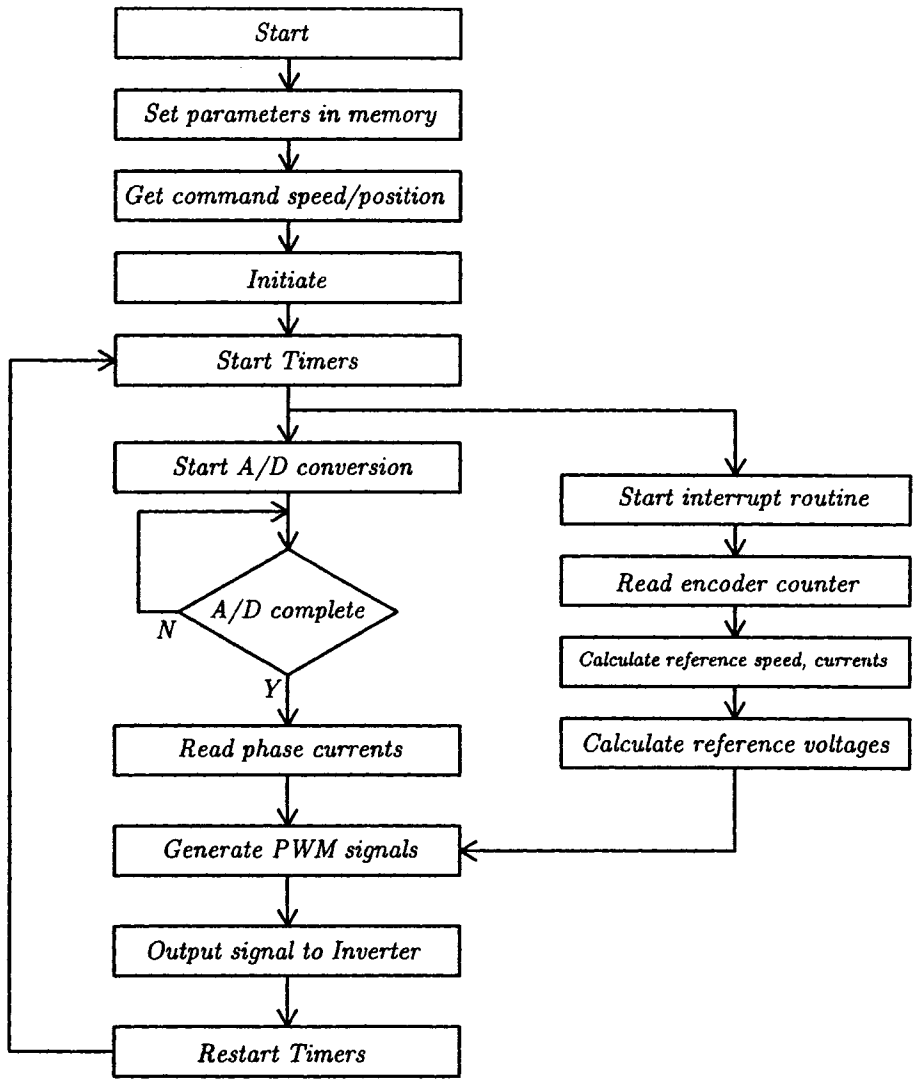

Figure 5.2: Flow chart of the software for real time implementation of the ABNL controller based IPMSM drive.

routine is set up to read the values of the currents and rotor position angle every 100 μs. After initializing all the required variables, the speed is calculated from the present and past samples of the rotor position angle. For position control, the error between the command and actual rotor position is used to generate the command position. Then using the values of the measured currents, errors, and parameters, the command voltages are generated from the adaptive non linear backstepping based control algorithm. Then the command voltages are compared with high frequency (3 kHz) triagular wave to generate the PWM signals.

Chapter 6

Conclusion

Based on the works reviewed in Chapter 1 and simulation studies presented in this thesis, it is concluded that the IPMSM can be used for variable speed high performance electric motor drives. This performance depends on the types of controllers used. Fixed gain types suffer from overshoot, undershoot and steady-state error. Some adaptive controllers require complex algorithms, as well as accurate system model parameters. It was found that adaptive backstepping based controllers gave very good speed performances with DC, induction and synchronous motors. However, it was found that an adaptive backstepping based position controller had not been developed for an IPMSM drive system. The vector control technique was used since the decoupled nature of the torque and flux allowed the IPMSM to be controlled like a DC motor.

In Chapter 2 the mathematical model of the IPMSM was derived in the synchronously rotating reference frame. Park's transformation was used to convert the conventional *abc* parameters to the synchronously rotating *dq* frame. It was clear that the q-axis current controlled the torque, and the d-axis current controlled the flux. The motor model was expressed in state space form for

simulation purposes and for control design.

In Chapter 3 the adaptive backstepping based controller was developed for speed and position control of an IPMSM. The motor model equations provided the basis for the design. Stability was proven using Lyapunov's Stability theory. The simulation model for the complete drive system and simulation results were shown in Chapter 4. The performance of both controllers was investigated at different operating conditions such as sudden change in command speed, load and parameter variation. It was found from the results that the proposed controller is robust and could be a potential candidate for high performance industrial drive applications. Both adaptive controllers were also compared with conventional fixed gain PI controllers and it was found that the performance of both ABNL based controllers are superior to the PI controllers.

6.1 Future Scope

As can be seen in Chapter 5, the real time implementation of the complete drive system has not been completed yet due to time constraints. This is the next logical step in this work. Also, more research studies are being reported using the speed sensorless approach [47, 48]. This will eliminate the need for a position encoder as well as any difficulties associated with it. Another technique which should be employed is the field weakening technique for wide speed range operation. Both speed and position controllers employed the technique of setting i_d to zero, which allows the motor to be controlled up to the rated speed. For control beyond rated speed, the field weakening technique must be used to calculate the command d-axis current.

Appendix A

IPMSM Parameters and Extra Equations

A.1 IPMSM Parameters

Number of phases = 3

Number of poles = 4

Rated Frequency = 60 Hz

Rated power = 1 HP

Rated input line-to-line voltage = 208 V

q-axis inductance $L_q = 0.07957H$

d-axis inductance $L_d = 0.04244H$

Stator resistance per phase $R = 1.93\,\Omega$

Inertia constant $J = 0.003\,kg \cdot m^2$

Rotor damping constant $B_m = 0.0008\,N \cdot m/rad/sec$

Permanent magnet flux linkage $\psi_m = 0.314\,volts/rad/sec$

A.2 Position Control Design Parameters

The following are the values of Φ_{1-6} as described in section 3.2.

$$\Phi_1 = \frac{-Ri_q - P\omega_r L_d i_d - P\omega_r \psi_m}{L_q} \tag{A.1}$$

$$\Phi_2 = \frac{-Ri_d + P\omega_r L_q i_q}{L_d} \tag{A.2}$$

$$\Phi_3 = (1 - k_1^2)e_1 + (k_1 + k_2)e_2 + \ddot{\theta}^* - \hat{C} - \hat{D}\omega_r \tag{A.3}$$

$$\begin{aligned}\Phi_4 = \frac{1}{A}[&(1 - k_1^2)(-k_1 e_1 + e2) + \\ &(k_1 + k_2)(-e_1 - k_2 e_2) + \theta^{(3)*} - \dot{\hat{D}} - \hat{D}^2\omega_r \\ &-\dot{\hat{C}} - \hat{C}\hat{D} + (k_1 + k_2)e_3 - \hat{D}i_q - \Phi_1\end{aligned} \tag{A.4}$$

$$\Phi_5 = \frac{1}{A}\Phi_3(k_1 + k_2) \tag{A.5}$$

$$\Phi_6 = \frac{1}{A}(k_1 + k_2) \tag{A.6}$$

Appendix B

Simulink Simulation

The details of the subsystem blocks for the simulink schematic of the complete drive system as shown in Figures 4.2 and 4.17(a) are presented in this appendix. There are three main subsystem blocks for speed control, the controller subsystem (B.2), the inverter subsystem (B.3) and the motor subsystem (B.5). The controller subsystem implements the control algorithm equations derived in section 3.1 and generates the command voltages. From here, they are transformed into the *abc* frame using Park's transformation and then compared with a high frequency triangle wave to generate the PWM signals. The logic signals NA, NB and NC are then transformed back to the *dq* frame for input to the motor model. For position control, the same blocks were used except a user defined Matlab function was used for the entire control algorithm.

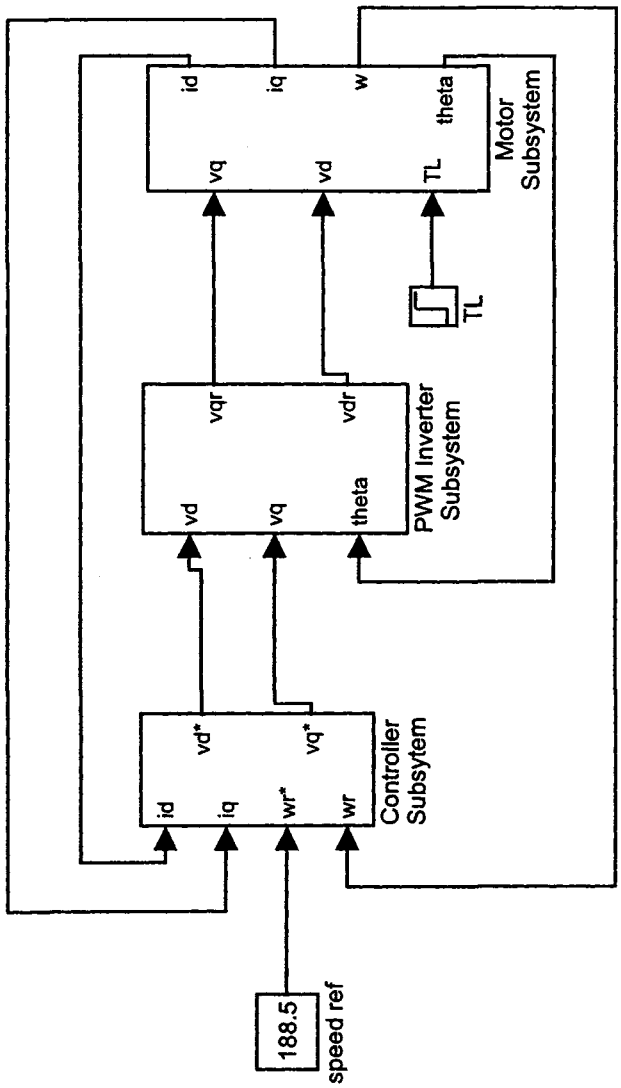

Figure B.1: Simulink schematic for speed control of IPMSM drive system

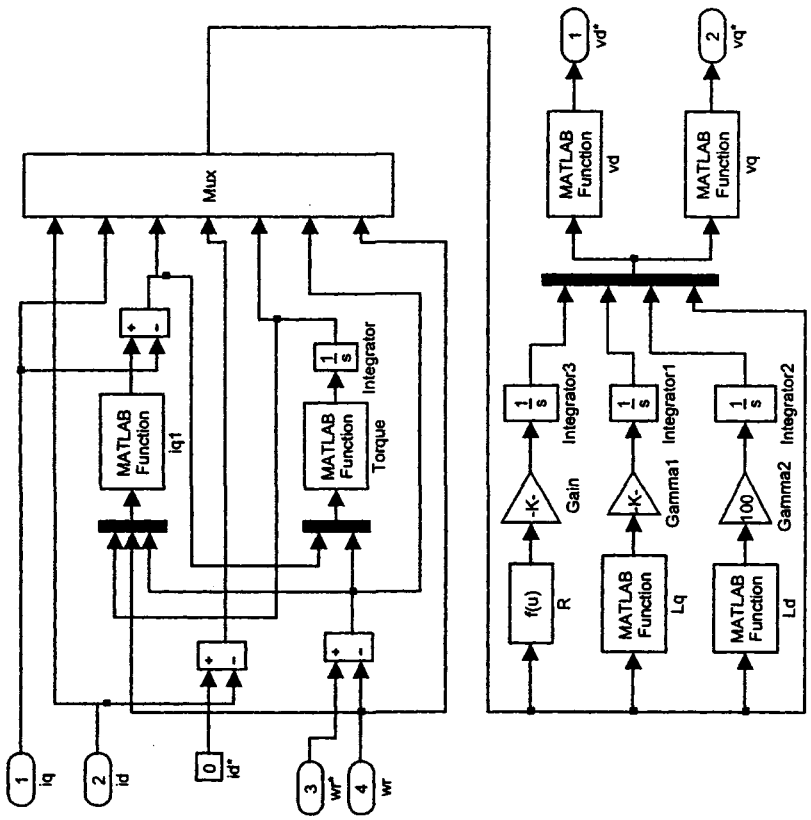

Figure B.2: Speed controller Subsystem

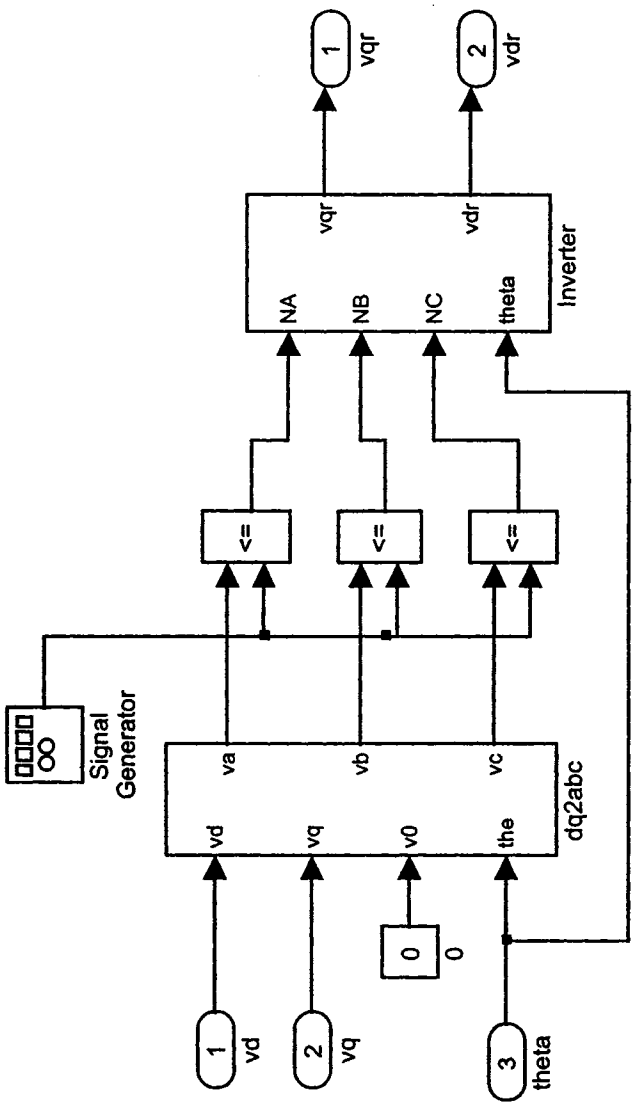

Figure B.3: PWM Inverter Subsystem

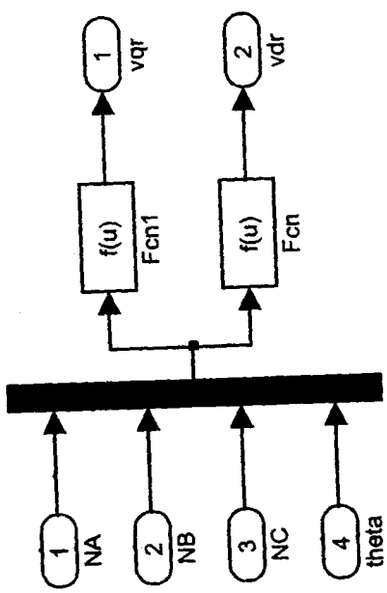

Figure B.4: Inverter Subsystem

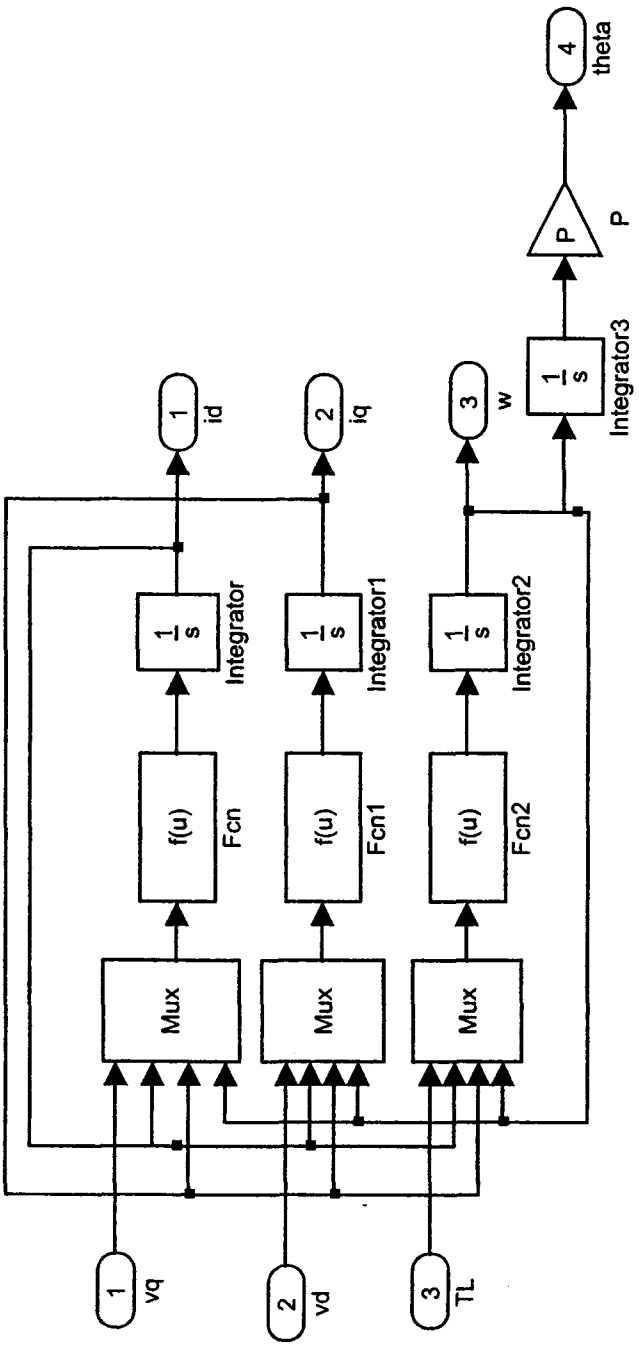

Figure B.5: Motor Subsystem

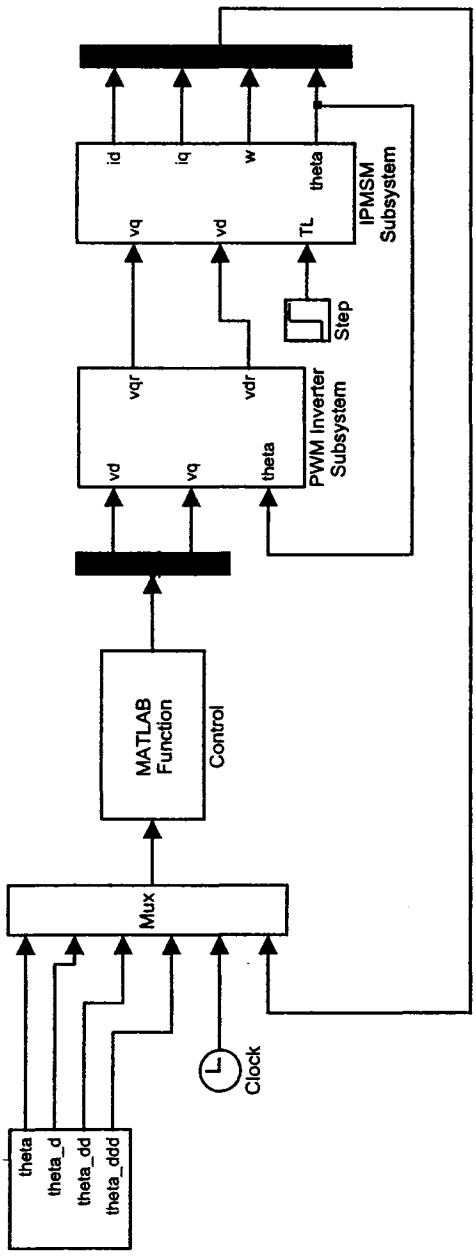

Figure B.6: Simulink model for position control

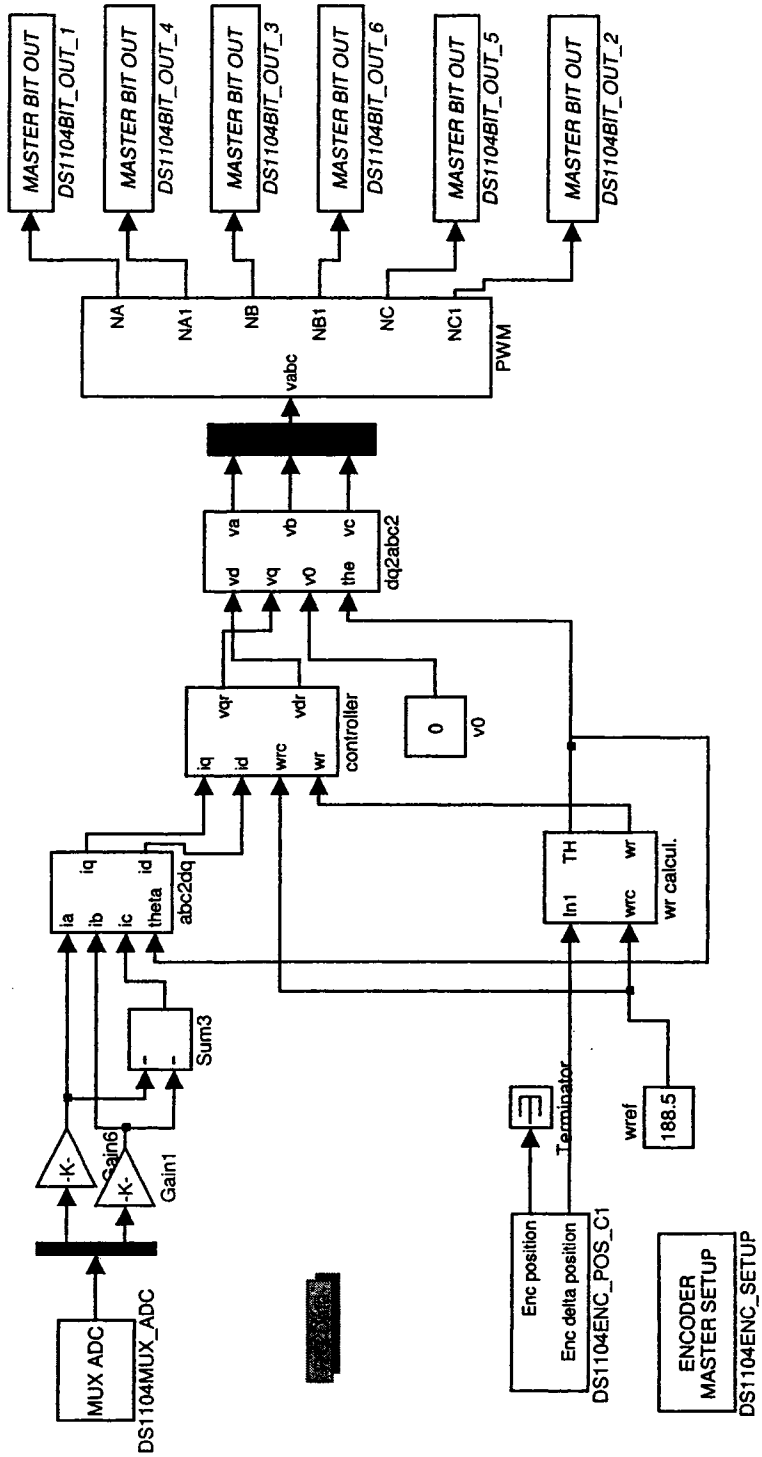

Figure B.7: Real-time Simulink model for speed control

Bibliography

[1] M. A. Rahman and P. Zhou, "Analysis of brushless permanent magnet synchronous motors," *IEEE Transactions on Industrial Electronics*, vol. 43, no. 2, pp. 256–267, Apr. 1996.

[2] B. K. Bose, *Modern Power Electronics and AC Drives.* Upper Saddle River, NJ: Prentice Hall, 2002.

[3] S. J. Chapman, *Electric Machinery Fundamentals.* New York, NY: McGraw-Hill, 1999.

[4] G. R. Slemon, *Electric Machines and Drives.* Reading, MA: Addison-Wesley, 1992.

[5] J. F. Gieras and M. Wang, *Permanent Magnet Motor Technology.* New York, NY: Marcel Dekker, Inc, 2002.

[6] A. Consoli and A. Raciti, "Analysis of permanent magnet synchronous motors," *IEEE Transactions on Industry Applications*, vol. 43, no. 2, pp. 350–354, Mar./Apr. 1991.

[7] G. Kang, J. Hong, and G. Kim, "Nonlinear characteristic analysis of interior type permanent magnet synchronous motor," in *Conf. Rec. Electric Machines and Drives*, vol. 1, 1999, pp. 69–71.

[8] U. Deshpande, "Recent advances in materials for use in permanent magnet machines - a review," in *Conf. Rec. IEEE Electric Machines and Drives Conference*, vol. 2, 2003, pp. 509–515.

[9] F. Blashke, "The principle of field orientation as applied to the new transvector closed loop control system for rotating field machines," *Siemens Review*, vol. 34, pp. 217–220, May 1972.

[10] R. H. Park, "Two-reaction theory of synchronous machines - generalized method of analysis part 1," *AIEE Transactions*, vol. 48.

[11] R. Marino, S. Peresada, and P. Valigri, "Adaptive input-output linearizing control of induction motors," *IEEE Transactions on Automatic Control*, vol. 38, no. 2, pp. 208–221, Feb. 1993.

[12] R. Ortega, P. Nicklasson, and G. Espinosa, "Passivity-based control of the general rotating electrical machines," in *Proc. IEEE Conf. Decision and Control*, 1994, pp. 4018–4023.

[13] K. R. Shouse and D. Taylor, "A digital self-tuning tracking controller for permanent-magnet synchronous motors," in *Proc. IEEE Conf. on Decision and Control*, vol. 4, 1993, pp. 3397–3402.

[14] E. Cerruto, A. Consoli, A. Raciti, and A. Testa, "A robust adaptive controller for pm motor drives in robotic applications," *IEEE Transactions on Power Electronics*, vol. 10, no. 1, pp. 62–71, Jan. 1995.

[15] M. Ghribi, H. Le-Huy, P. Viarouge, and L. Dessaint, "Adaptive position control of a permanent magnet synchronous motor drive," in *Conf. Rec. IEEE-IAS Annual Meeting*, vol. 1, 1990, pp. 647–652.

[16] R. B. Sepe and J. Lang, "Real-time adaptive control of the permanent-magnet synchronous motor," *IEEE Transactions on Industry Applications*, vol. 27, no. 4, pp. 706–714, July/Aug. 1991.

[17] ——, "Real-time observer-based (adaptive) control of a permanent-magnet synchronous motor without mechanical sensors," *IEEE Transactions on Industry Applications*, vol. 28, no. 6, pp. 1345–1352, Nov./Dec. 1992.

[18] F. J. Lin and Y. S. Lin, "A robust pm synchronous motor drive with adaptive uncertainty observer," *IEEE Transactions on Energy Conversion*, vol. 14, no. 4.

[19] X. Yue, D. Vilathgamuwa, and K. Tseng, "Observer-based robust adaptive control of pmsm with initial rotor position uncertainty," *IEEE Transactions on Industry Applications*, vol. 39, no. 3, pp. 645–656, May/June 2003.

[20] K. K. Shyu, C. Lai, Y. Tsai, and D. Yang, "A newly robust controller design for the position control of permanent magnet synchronous motor," *IEEE Transactions on Industrial Electronics*, vol. 49, no. 3, pp. 558–565, June 2002.

[21] F. M. Freitas-Sa, Z. Peixoto, P. Seixas, B. Menezes, P. Cortizo, and W. Lacerda, "An interior permanent magnet synchronous motor position control using sliding mode," in *Conf. Rec. International Conference on Power Electronics and Drive Systems*, vol. 2, 1995, pp. 593–598.

[22] S. Brock, J. Deskur, and K. Zawirski, "Robust speed and position control of pmsm," in *Proc. IEEE International Symposium on Industrial Electronics*, vol. 2, 1999, pp. 667–672.

[23] V. Petrovic, R. Ortega, A. M. Stankovic, and G. Tadmor, "Design and implementation of an adaptive controller for torque ripple minimization in pm synchronous motors," *IEEE Transactions on Power Electronics*, vol. 15, no. 5, pp. 871–880, Sept. 2000.

[24] R. S. Colby and D. W. Novotny, "An efficiency-optimizing permanent-magnet synchronous motor drive," *IEEE Transactions on Industry Applications*, vol. 24, no. 3, pp. 462–469, May/June 1988.

[25] S. Morimoto, K. Hatanaka, Y. Tong, Y. Takeda, and T. Hirasa, "Servo drive system and control characteristics of salient pole permanent magnet synchronous motor," *IEEE Transactions on Industry Applications*, vol. 29, no. 2, pp. 338–343, Mar./Apr. 1993.

[26] L. Salvatore and S. Stasi, "Adaptive position control of a pmsm drive," in *Conf. Rec. IECON Industrial Electronics, Control and Instrumentation*, vol. 3, 1994, pp. 2079–2085.

[27] M. Ghribi and H. Le-Huy, "Optimal control and variable structure combination using a permanent-magnet synchronous motor," in *Conf. Rec. IEEE-IAS Annual Meeting*, vol. 1, 1994, pp. 408–415.

[28] B. Zhang and Y. Li, "A pmsm sliding mode control system based on model reference adaptive control," in *Proc. PIEMC Power Electronics and Motion Control Conference*, vol. 1, 2000, pp. 336–341.

[29] J. Zhou, Y. Wang, and R. Zhou, "Adaptive backstepping control of separately excited dc motor with uncertainties," in *Conf. Rec. International Conf. on Power System Technology*, vol. 1, 2000, pp. 91–96.

[30] H. Tan and J. Chang, "Adaptive backstepping control of induction motor with uncertainties," in *Conf. Rec. American Control Conference*, vol. 1, 1999, pp. 1–5.

[31] H. Tan, "Field orientation and adaptive backstepping for induction motor control," in *Conf. Rec. IEEE-IAS Annual Meeting*, vol. 4, 1999, pp. 2357–2263.

[32] H. Tan and J. Chang, "Adaptive position control of induction motor systems under mechanical uncertainties," in *Conf. Rec. IEEE International Conf. on Power Electronics and Drive Systems*, vol. 2, 1999, pp. 597–602.

[33] C. I. Huang, K. L. Chen, H. T. Lee, and L. C. Fu, "Nonlinear adaptive backstepping motion control of linear induction motor," in *Conf. Rec. American Control Conference*, vol. 4, 2002, pp. 3099–3104.

[34] D. F. Chen, T. H. Liu, and C. K. Hung, "Nonlinear adaptive-backstepping controller design for a matrix-converter based pmsm control system," in *Conf. Rec. IEEE-IES Annual Meeting*, vol. 1, 2003, pp. 673–678.

[35] J. Zhou and Y. Wang, "Adaptive backstepping speed controller design for a permanent magnet synchronous motor," in *IEE Proceedings in Electric Power Applications*, vol. 149, 2002, pp. 165–172.

[36] M. Vilathgamuwa, M. A. Rahman, K. Tseng, and M. N. Uddin, "Nonlinear control of interior permanent magnet synchronous motor," *IEEE Transactions on Industry Applications*, vol. 39, no. 2, pp. 408–415, Mar./Apr. 2003.

[37] M. E. Haque and M. F. Rahman, "Influence of stator resistance variation on direct torque controlled interior permanent magnet synchronous motor drive performance and its compensation," in *Conf. Rec. IEEE-IAS Annual Meeting*, vol. 4, 2001, pp. 2563–2569.

[38] M. N. Uddin, "Intelligent control of an interior permanent magnet synchronous motor," Ph.D. dissertation, Memorial University of Newfoundland, St. John, Oct. 2000.

[39] S. Morimoto, M. Sanda, and Y. Takeda, "Effects and compensation of magnetic saturation in flux-weakening controlled permanent magnet synchronous motor drives," *IEEE Transactions on Industry Applications*, vol. 30, no. 6, pp. 1632–1637, Nov./Dec. 1994.

[40] M. F. Rahman, L. Zhang, and K. W. Lim, "A direct torque-controlled interior permanent magnet synchronous motor drive incorporating field weakening," *IEEE Transactions on Industry Applications*, vol. 34, no. 6, pp. 1246–1253, Nov./Dec. 1998.

[41] P. Pillay and R. Krishnan, "Control characteristics and speed controller design for high performance permanent magnet synchronous motor drives," *IEEE Transactions on Power Electronics*, vol. 5, no. 2, pp. 151–159, Apr. 1990.

[42] M. Uddin and J. Lau, "Adaptive backstepping based nonlinear control of an ipmsm drive," in *Power Electronic Society Conference, Aachen Germany*, 2004, pp. 3451–3457.

[43] I. K. M. Kristic and P. Kokotovic, *Nonlinear and Adaptive Control Design.* New York, NY: John Wiley and Sons, 1995.

[44] J. Lau and M. N. Uddin, "Non linear adaptive back stepping based control for ipmsm drive," in *International Electric Machines and Drives Conference, San Antonio TX, USA*, 2005, pp. 1689–1694.

[45] Matlab, *Simulink User Guide.* The Mathworks Inc., 2004.

[46] dSPACE, *Implementation Guide.* Germany: Paderborn, 2003.

[47] S. Ostlund and M. Brokemper, "Sensorless rotor-position detection from zero to rated speed for an integrated pm synchronous motor drive," *IEEE Transactions on Industry Applications*, vol. 32, no. 5, pp. 1158–1165, Sept./Oct. 1996.

[48] L. Tang, L. Zhong, M. Rahman, and Y. Hu, "A novel direct torque control for interior permanent-magnet synchronous machine drive with low ripple in torque and flux-a speed-sensorless approach," *IEEE Transactions on Industry Applications*, vol. 39, no. 6, pp. 1748–1756, Nov./Dec. 2003.